1

AIR FORCE INSTITUTE OF TECHNOLOGY

AIR UNIVERSITY
UNITED STATES AIR FORCE

AN INVESTIGATION OF THE GAMMA PHASE OF THE TITANIUM-ALUMINUM BINARY ALLOY WITH ZIRCONIUM ADDITIONS

by
Duane H. Troup
Major USAF

GAW/Mech 62-16

SCHOOL OF ENGINEERING

WRIGHT-PATTERSON AIR FORCE BASE, OHIO

AN INVESTIGATION OF THE GAMMA PHASE OF THE TITANIUM-ALUMINUM BINARY ALLOY WITH ZIRCONIUM ADDITIONS

by
Duane H. Troup
Major USAF

GAW/Mech 62-16

THESIS

Presented to the Faculty of the School of Engineering of

the Air Force Institute of Technology

Air University

in Partial Fulfillment of the

Requirements for the Degree of

Master of Science

AN INVESTIGATION OF THE GAMMA PHASE OF THE TITANIUM-ALUMINUM BINARY ALLOY WITH ZIRCONIUM ADDITIONS

by
Duane H. Troup
Major USAF

GAW/Mech 62-16

Graduate Aeronautical Engineering

August 1962

Preface

The results of a study to determine the extent of solubility of zirconium in the gamma phase of the titanium-aluminum binary alloy are presented herein. Previous work in this field was considered when the final analysis was made and the conclusions drawn.

I wish to express my appreciation to Mr. Craig Hartley, Project Engineer, High Temperature Section, Physical Metallurgy Branch, Materials Central, ASD, for his advice, help in specimen preparation and analysis, and for the use of the ASD furnace and vacuum pump employed in this work. Special thanks are due Major Edward J. Myers, metallurgy instructor at AFIT and thesis advisor for this study, for his guidance and counselling, and for his encouragement during the course of this investigation.

I would also like to express my gratitude to my wife, without whose help this report would not have been completed.

Duane H. Troup

Contents

Contents

List of Figures

List of Tables

List of Symbols

Symbol	Definition
a	-Length of base of crystal
c	-Height of crystal
c/a	-Ratio of height of crystal to base
w/o	-Weight percent
a/o	-Atomic percent
θ	-Angle at which planes of atoms reflected x-rays
λ	-Wave length of x radiation
α_2	-Ti_2Al phase
γ	-Equiatomic TiAl phase
ϕ	-Phase appearing in Specimen 12 (35a/o Ti, 55a/o Al, 10a/o Zr)

Abstract

The titanium-aluminum equiatomic alloy has qualities of excellent corrosion resistance, good strength to weight ratio, and good hot hardness. These qualities would make this alloy a desirable structural material were it not for an inherent brittleness and lack of ductility.

The brittleness is attributed to an ordered-face-centered-tetragonal cell with a c/a ratio of 1.020. Several attempts have been made to reduce the c/a ratio to unity through ternary additions. A reduction of this ratio to 1.006 has been reported with zirconium as the ternary addition; however, this value was attained outside of the gamma phase.

During this investigation the limit of solubility of zirconium in the gamma phase at 2325°F was determined to be slightly less than 10a/o at 55a/o aluminum and slightly more than 10a/o at 60a/o aluminum. The c/a ratio varied with composition from 1.016 to 1.030.

GAW/Mech 62-16

AN INVESTIGATION OF THE GAMMA PHASE OF THE TITANIUM-ALUMINUM BINARY ALLOY WITH ZIRCONIUM ADDITIONS

I. Introduction

The use of titanium as a structural material has been of great interest for the last fifteen years because of its desirable properties of corrosion resistance and high strength to weight ratio. Various binary elements have been alloyed with titanium to improve these properties but only aluminum additions result in a structurally useful alloy with significantly lower density. Aluminum additions also improve oxidation resistance and the equiatomic (gamma phase) Ti-Al alloy has the most outstanding oxidation resistance of all known binary titanium base alloys (Ref 10). Another advantage of the gamma phase is that it exists over a large temperature and solubility range (Fig. 1).

H. D. Kessler and J. B. McAndrew, working for the Armour Research Foundation, conducted an investigation of the gamma phase alloy (Ref 9). Their results indicated good hot hardness with superior oxidation and corrosion resistance at both low and elevated temperatures. However, these advantages are offset by brittleness exhibited at room and elevated temperatures. This brittleness is attributed to the ordered arrangement of atoms on the face-centered tetragonal cell where (001) planes of titanium

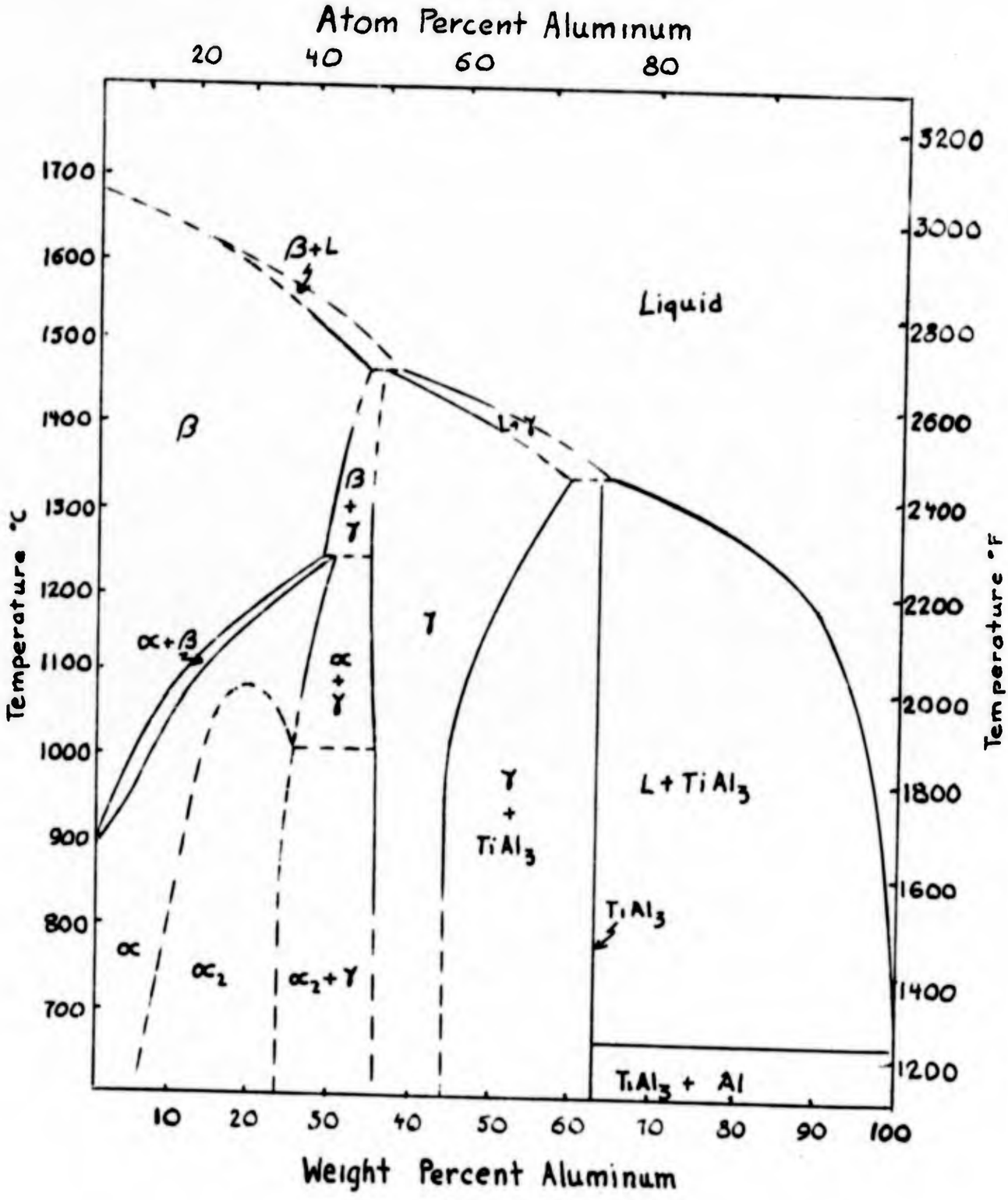

(Ref 10:12)

Fig. 1
Tentative Ti-Al Phase Diagram

atoms alternate with like planes of aluminum atoms (see Appendix A). The c/a ratio of this tetragonal crystal is 1.020.

Kessler and McAndrew tried to reduce the c/a ratio to unity by ternary additions of 13 different elements. They expected the atoms to become disordered as the crystal became cubic with an accompanying decrease in the brittleness of the alloy. They did manage to achieve a c/a ratio of 1.012 but were unable to get a further reduction.

In 1959, Davies investigated the Ti-Al system and reported a reduction of the c/a ratio to 1.006 when he replaced 15a/o of titanium with a like amount of zirconium. However, Davies did not determine the phases present and a later work indicated that he was outside of the gamma phase when this low c/a ratio was obtained (Ref 13).

Sandlin and Klung worked with 27 compositions of aluminum, titanium, and zirconium in a subsequent investigation (Ref 13). A few of their specimens were similar to those studied by Davies, but they were unable to duplicate his results. They determined that Davies was in a multi-phase region when he measured a c/a ratio of 1.006. The minimum value of the c/a ratio measured by Sandlin in the gamma phase was 1.016. The boundary of the gamma phase region at 2000°F as determined by Sandlin is shown in Fig. 5. In preparing his specimens for the phase investigation, Sandlin heat treated them at 2000°F for 36 to 39 hours. The specimens were air cooled after this homogenization.

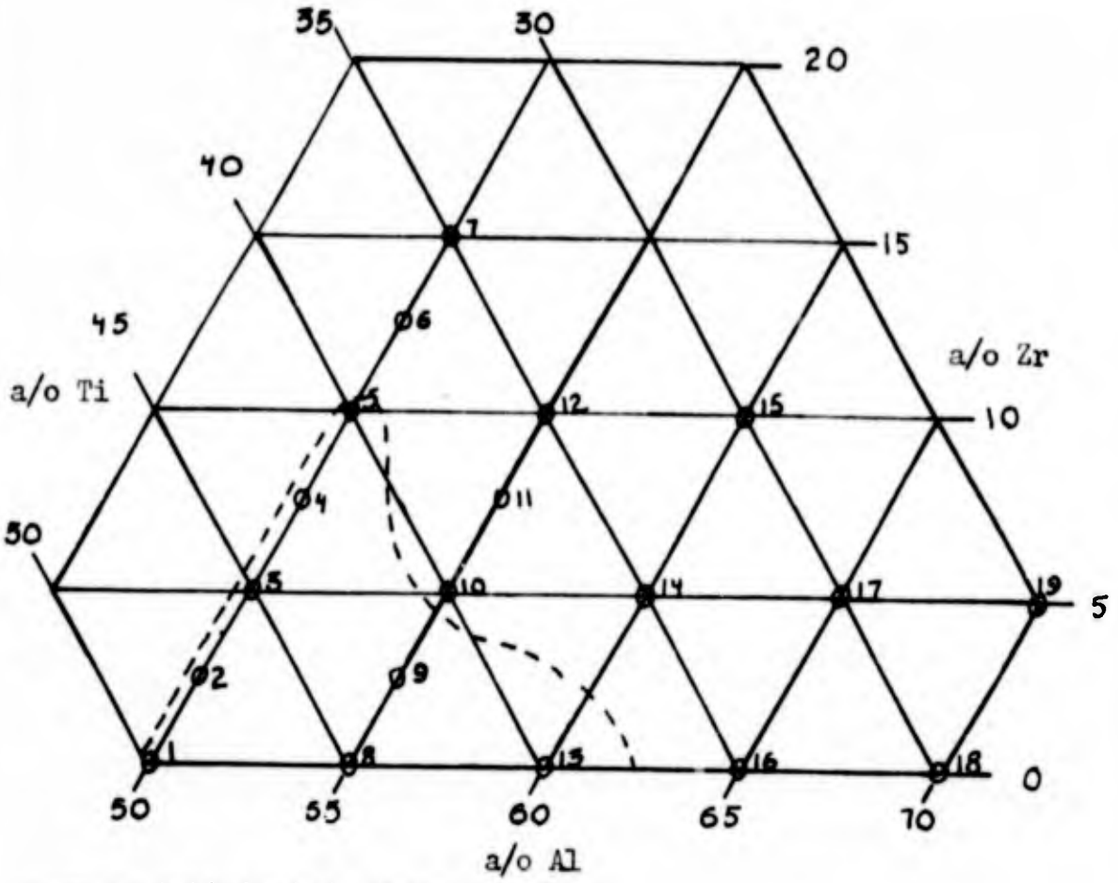

— — — Anticipated Phase Boundary

o Compositions selected for investigation

Fig. 2

Nominal Composition

and

Expected Phase Boundary

The purpose of this investigation was to determine:

1) the extent of the gamma phase in the Ti-Al-Zr alloy and

2) the variation of the c/a ratio with composition in that phase.

The nominal composition of the alloys used are shown in Fig. 2 and are also listed in Table V. The dashed line in Fig. 2 represents the anticipated limit of the gamma phase and the specimen compositions were chosen so as to include this region.

The specimens considered in this investigation were examined under normal, tinted, and polarized light on the metallograph and the same portion of each specimen was investigated by x-ray diffraction. The conclusions are based primarily on the diffraction patterns.

The experimental procedure, analyses of data, and the conclusions will follow in that order. The data and pictures of representative samples are included in the appendices.

II. Experimental Procedure

Preparation of Specimens

High purity elements (aluminum from the Aluminum Co. of America, sponge titanium from the U. S. Bureau of Mines, and zirconium from the Reaction Metals Corporation) were examined spectrographically by the Bowser-Morner Testing Laboratories, Inc. of Dayton, Ohio. The results of their analysis are listed in Table I.

TABLE I

Impurities in Alloying Elements

Note: 1) Values are in weight percent
2) $<$ is used to signify "less than"

Impurity	Aluminum	Titanium	Zirconium
Silicon	.01	$<$.01	$<$.01
Manganese	$<$.003	.02	$<$.01
Copper	.002	$<$.01	$<$.01
Iron	.02	$<$.01	$<$.01
Magnesium	$<$.002	$<$.01	$<$.01
Titanium	$<$.005	-	-
Nickel	$<$.01	$<$.01	$<$.01
Aluminum	-	$<$.01	$<$.01
Hafnium	-	-	.21

The three elements were broken into small pieces and weighed to the nearest 5 milligrams to obtain the desired atomic percentages.

The elements were then compressed together in a metallurgical specimen mounting press under a pressure of 10000 psi.

Melting of the alloys was accomplished in a Zak Button Furnace at the Research Institute of the University of Dayton. The furnace, an electric arc type, is a vacuum chamber with cylindrical walls and a water cooled copper hearth containing 5 depressions (crucibles) for melting the specimens. The power is supplied by a 30-volt, 600amp dc generator. The water cooled, tungsten-tipped, non-consumable electrode is fitted through a ball joint located at the top of the furnace. The ball joint fitting enables the operator to move the electrode over the five button crucibles.

Compacted specimens were placed in four of the crucibles and a pure titanium "getter" of 75 Brinell Hardness was placed in the fifth. The furnace was sealed and evacuated to one micron of pressure and then flushed with an inert atmosphere of helium and argon. The evacuating and flushing procedures were repeated several times to insure a non-reactive atmosphere in the chamber.

Titanium "getters" were used as deoxidizers to further insure a non-reactive atmosphere when the specimens were melted. With the exception of alloys 5, 6, 7, and 8, the specimens were melted 4 times. Approximately one gram of weight was lost by each sample during the melting operation. Specimens 5 through 8 were melted three times. Little difference in weight loss between

the samples melted 3 times and those melted 5 times was observed. The Brinell Hardness Number of the "getter" remained less than 80 during operations. This indicated an atmosphere relatively free of impurities as the hardness of titanium is directly related to impurities contained therein. Because of the weight loss, the samples were analysed and the results are contained in Appendix B.

An attempt was made to section the button-shaped specimens with a band saw. However, the saw was dulled and the sample became quite hot so the attempt was abandoned. The buttons were broken into small pieces by placing them on an anvil and pounding them with a hammer.

Pieces of each specimen, weighing between five and ten grams, were wrapped in tantalum foil and encapsulated in quartz at less than one micron of pressure. In several cases, an unwrapped piece of the specimen was encapsulated with the wrapped piece. The specimens were homogenized and a very slight oxide film was found on some of the unwrapped pieces but no film was discovered on any of the wrapped pieces. The oxide film was removed by pickling in a solution of 5% HF, 50% HNO_3, and 45% H_2O. The specimens were heat treated as shown in Table II.

Table II

Heat Treatment

Note: 1) All specimens were quenched by breaking the quartz under water.
2) The furnace was run at a constant power setting with the exception of the first run. The variation in temperature is due to power fluctuations and the average temperature is reported.

Specimen	Temperature	Time-hours
1,2	2515°F	23.6
3,4	2354°F	23.5
5,6	2348°F	24.0
7,8	2365°F	23.7
9,10	2368°F	23.8
11,12	2322°F	24.1
13	2286°F	24.0
14	2275°F	38.5
15,16	2283°F	25.5
17,18	2282°F	24.3
19	2278°F	29.2

Metallography

The annealed specimens were mounted in lucite for easy handling. A flat surface was ground on each with a belt sander and the flat surfaces were then polished with successively finer grades of paper to 4/0. After each grade of paper was used, the specimen was examined under a microscope to see that scratches from the previous grade of paper were removed. It was noticed that the surfaces were not becoming smooth, but rather, that small bits of the specimen were being pulled from the surface. Further polishing, even with very light pressure, did not improve the surfaces. An attempt was then made to polish the specimens on an electrically driven turntable using successively finer grades of alumina. The final polishing was done at low speed on a vibra-polisher with 1551 AB Gamma Polishing Alumina #3 as the abrasive. There was improvement in the surface of the alumina-polished specimens although most of the samples still contained the pits after 12 to 16 hours of polishing.

The specimens were etched with Kroll's etch (6% HNO_3, 3% HF, 91% H_2O) and photographed on a Bausch and Lonb Metallograph. Many of the specimens contained microscopic cracks which interferred with interpretation of the grain boundaries. The cracks were believed due to rapid quenching of the specimens. In addition, the bits of metal torn from the surface might have been a large grain or a different phase. Most of the specimens were sent to the University of Dayton Research Institute, Dayton, Ohio for

examination by their metallographer, Mr. E. P. Harich. He polished the specimens chemically and etched them with Kroll's etch. He returned specimens 15, 17, 18, and 19 as they were too cracked for metallographic study. In addition he polished and etched as-melted portions of the same specimens. Photomicrographs of representative specimens are located in Appendix G.

It is interesting to note that Mr. Harich also experienced similar difficulties in polishing the specimens. Even though extremely light pressure was used in the preliminary polishing, small bits of metal were pulled loose from the surface of the specimen. He also reported low angle grain boundaries, visible with both offset and polarized light but not with normal light.

X-ray Procedures

The specimens were removed from the lucite mounting for x-ray study. At first an attempt was made to drill powder from the center of the mounted sample for x-ray diffraction. This method was unsuccessful due to the hardness of the specimens. Therefore, the specimens were powdered in a mortar with a diamond-tipped pestle. The powder was made fine enough to pass through a 325 mesh screen.

The powder was wrapped in tantalum foil and encapsulated in vycor at a pressure of less than one micron. The encapsulated powders were given a heat treatment for stress relief as indicated in Table III.

TABLE III

Stress Relief

Note: All powders were heated at 1110°F for stress relief

Specimen	Time at Temperature Hours
1	1.0
2	2.5
3	1.0
4	5.0
5	2.5
6	5.0
7	1.0
8	2.5
9	5.0
10	2.5
11	2.5
12	5.0
13	1.0
14	5.0
15	5.0
16	5.0
17	5.0
18	2.5
19	5.0

After the stress relief, the powders were x-rayed on a North American Phillips X-ray Diffractometer composed of a water-cooled x-ray diffraction unit, a wide range goniometer, and a Brown strip chart recorder. Copper $K\alpha$ radiation (λ=1.54051A°) was used and the diffractometer was calibrated by scanning the peaks of a silicon standard specimen and comparing the observed values of 2θ with the published values. The diffractometer was calibrated three times during the investigation and the calibration correction is shown in Fig. 3.

Each powdered specimen was wrapped in a thin plastic film and placed in an aluminum holder in the middle of the goniometer. Scanning was accomplished in both directions over the range of 2θ from 16° to 162° at the rate of 2 degrees per minute with additional scans being taken of doubtful areas as necessary. The patterns of each specimen were superimposed on a light table and compared. In this manner the very weak peaks could be separated from the normal variations in intensity as the reflections from planes of atoms were consistent in location on both charts while the rest of the pattern was not. This method of comparison was also used in determining a change in the diffraction patterns between specimens. Specimen eight (45a/o Ti, 55a/o Al) was identified by comparison with published data (Ref 6) and all other specimens were compared with No. 8. The $TiAl_3$ phase was identified by comparison with the values published in the X-ray Powder Diffraction File (Ref 14) and the Ti_2Al phase (α_2) was compared with the work of Ence and Margolin (Ref 7) for identification. A list of the reflecting planes with their identification and relative intensities is located in Appendix D.

The peaks of each alloy between 65° and 162° were scanned in both directions at a slower speed so a more precise angle could be measured. Specimens 10, 11, 14, and 16 were scanned at 1/2 degree per minute and the others were scanned at 1/4 degree per minute. A chart speed of 1/2 inch per minute allowed reading the angles

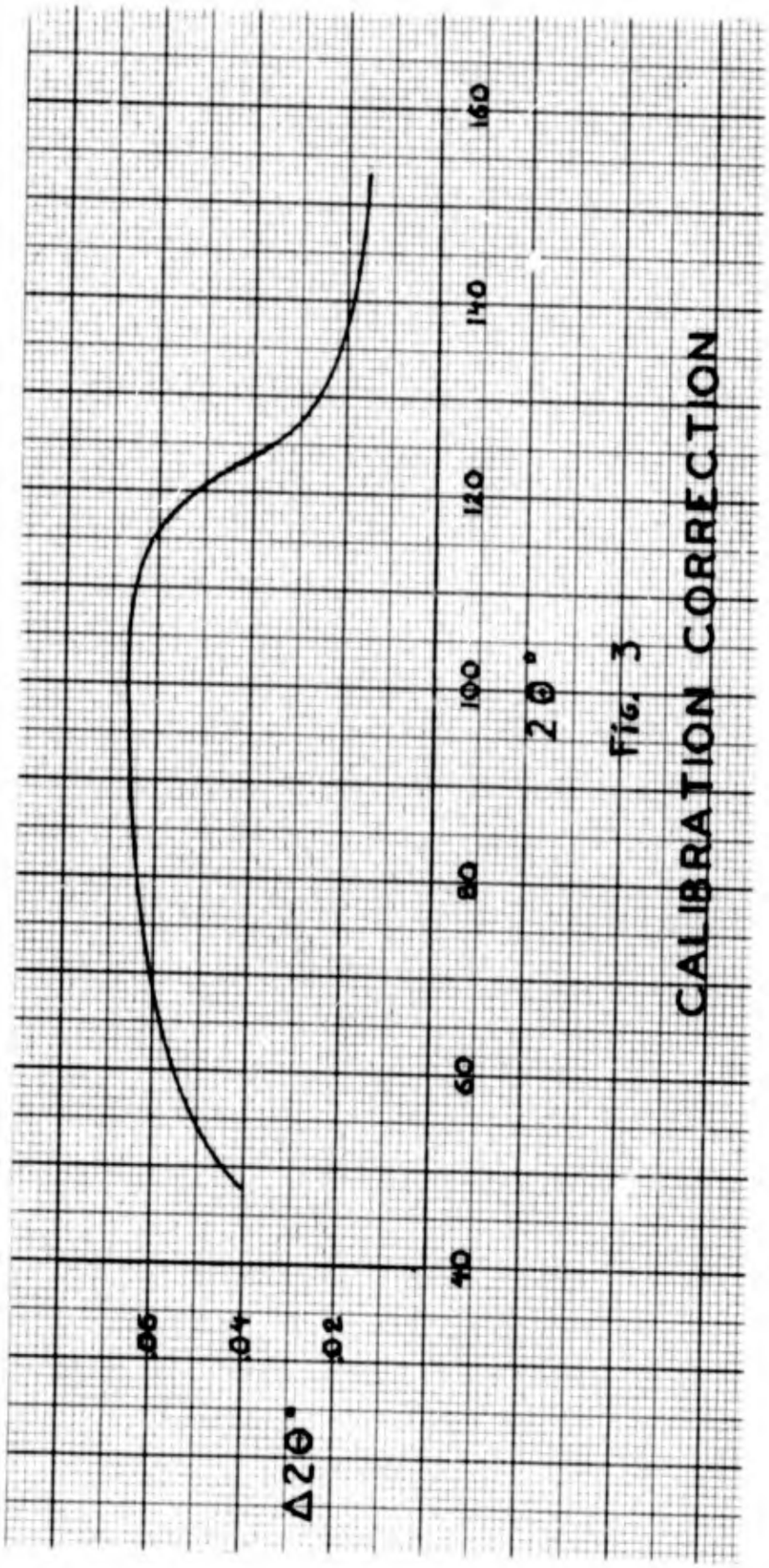
CALIBRATION CORRECTION
Fig. 3
2θ°
160
140
120
100
80
60
40
Δ2θ°
.06
.04
.02

of the reflections at the faster speed to the nearest 0.01 degree and those at the slower speed to the nearest 0.005 degree. The use of an engineer's rule with 100 graduations per inch made even more precise measurements possible but all values of 2θ were rounded to the nearest 0.01 degree. The values of 2θ for the more intense reflections were used in determining the lattice parameters of the gamma phase.

The lattice parameters were determined graphically by a method devised by Myers and Davies (Ref 11). The tabulations of data for the graphical solutions are contained in Appendix E and the graphical solutions are located in Appendix F.

III. Analyses of Data

Phase Determination

The determination of phases present in each alloy was based upon the reflections in the range of 2θ values to 90°. In the back reflection region the peaks were quite diffuse and zirconium fluorescence in the ternary alloys made the analyses difficult. Zirconium fluorescence is a term used to describe x-rays emitted by the zirconium atoms returning from an excited state to the normal or ground state. Some of the copper radiation was absorbed by the zirconium and this energy raised the atoms to an excited state (Ref 1:45-68). This fluorescent radiation was picked up by the Geiger Counter resulting in increased background intensity.

Before any of the patterns were indexed, the two or more scans from each specimen were compared by superimposing the more intense peaks. The position of the 2θ values of the reflection plane could vary between a forward and a backward scan but the distance between peaks for any one specimen remains constant. In this manner the weaker peaks could be picked from the background clutter. Any change in intensity that remained constant from one scan to the next was assumed to be caused by a reflecting plane and was so listed.

The x-ray pattern of alloy eight (45a/o Ti, 55a/o Al) was indexed by comparing it with the results of work by Duwez and Taylor (Ref 6). Only peaks of the gamma phase appeared in the

diffraction pattern and therefore this specimen was used to identify the gamma phase in the other alloys.

The patterns of the seven specimens containing 50a/o aluminum contained reflections identified as Ti_2Al (α_2) in addition to those identified as gamma phase. The peaks of the gamma phase were much stronger than those of the α_2 phase indicating that the composition was primarily γ.

The four specimens containing 55a/o aluminum were then compared with the gamma phase. Specimens 9 (42.5a/o Ti, 2.5a/o Zr), 10 (40a/o Ti, 5a/o Zr), and 11 (37.5a/o Ti, 7.5a/o Zr) each had a weak reflection that was not repeated in the other specimens. The peak in alloy nine was at 40.9°, that in alloy 10 was at 114.9°, and the one in alloy 11 was at 94.2°. These peaks were not identified as either α_2 or $TiAl_3$. Specimens 12 (35a/o Ti, 55a/o Al, 10a/o Zr) contained some very weak peaks at 2θ values of 27.6°, 33.1°, 36.3°, 41.4°, 42.6°, 84.6°, 128.7°. Although these peaks were identified as belonging to a new phase, ϕ, they approximate the α_2 pattern quite closely.

The three alloys containing 60a/o aluminum, specimens 13 (40a/o Ti), 14 (35a/o Ti, 5a/o Zr), 15 (30a/o Ti, 10a/o Zr), were compared with each other and determined to be of the same phase. Again each of the three had a very weak reflection that was not present in the patterns of the other two. In this case, there is some doubt as to the actual existance of reflecting planes and they are listed because there was a slight increase in intensity

in the same relative position on both scans. This was the criterion for selecting the weak peaks as mentioned before. After determining that these three specimens were of the same phase (or phases) they were compared with specimen eight (45a/o Ti, 55a/o Al) and found to be single phase γ.

The same procedure was followed for the two alloys containing 65a/o aluminum. Four peaks of specimen 16 (35a/o Ti, 65a/o Al) and 7 peaks of specimen 17 (30a/o Ti, 65a/o Al, 5a/o Zr) were identified as $TiAl_3$. Two very weak reflections in specimen 16, one at 95.9° and the other at 100.3° were unidentified. The rest of the peaks were identified as gamma phase. A weak peak at 35.0° 2θ and four in the back reflection region of alloy 17 were unidentified. They correspond neither to the gamma phase nor to the $TiAl_3$ phase. The rest of the peaks fit the pattern of the gamma phase.

Specimens 18 (30a/o Ti, 70a/o Al) and 19 (25a/o Ti, 70a/o Al, 5a/o Zr) were identified as a mixture of gamma and $TiAl_3$.

Graphs showing the variation of the reflecting planes of the gamma phase are contained in Appendix B. In general, the 2θ values of reflecting planes decrease with increasing zirconium content and increase slightly or remain constant with increasing aluminum content.

The results of this investigation indicate that the gamma phase extends into ternary alloy to slightly more than 10a/o zirconium at an aluminum content of 60a/o, and to slightly less

than 10a/o zirconium with an aluminum content of 55a/o. The results of Sandlin's investigation show the limit of the gamma phase to be just short of 9.2a/o with an aluminum content of 52.2a/o and titanium content of 38.6a/o. This variation is not unexpected and shows that the gamma phase has a greater solubility for zirconium at higher temperatures. The same situation exists in the binary Ti-Al alloy on the aluminum-rich side. Here the increase in the solubility of aluminum between 2000°F and 2200°F is on the order of 5a/o.

Determination of Lattice Parameters in χ Phase

Diffraction patterns were taken of specimens 8 through 15 for use in determining the lattice parameters. The five peaks in the higher ranges of 2θ with the strongest intensity were selected for this purpose. Peaks of specimens 8, 9, 12, 13, and 15 were scanned in both directions at the rate of one-fourth degree per minute. Peaks of specimens 10, 11, and 14 were scanned at one-half degree per minute. The values of the 2θ angles for each peak were averaged together and corrected for calibration error. Myers' and Davies' graphical method of precise lattice parameter determination (Ref 11) was used to analyse all data.

Table IV contains the lattice parameter determination from this study and Fig. 4 shows the comparison of these results with those of Sandlin and Davies.

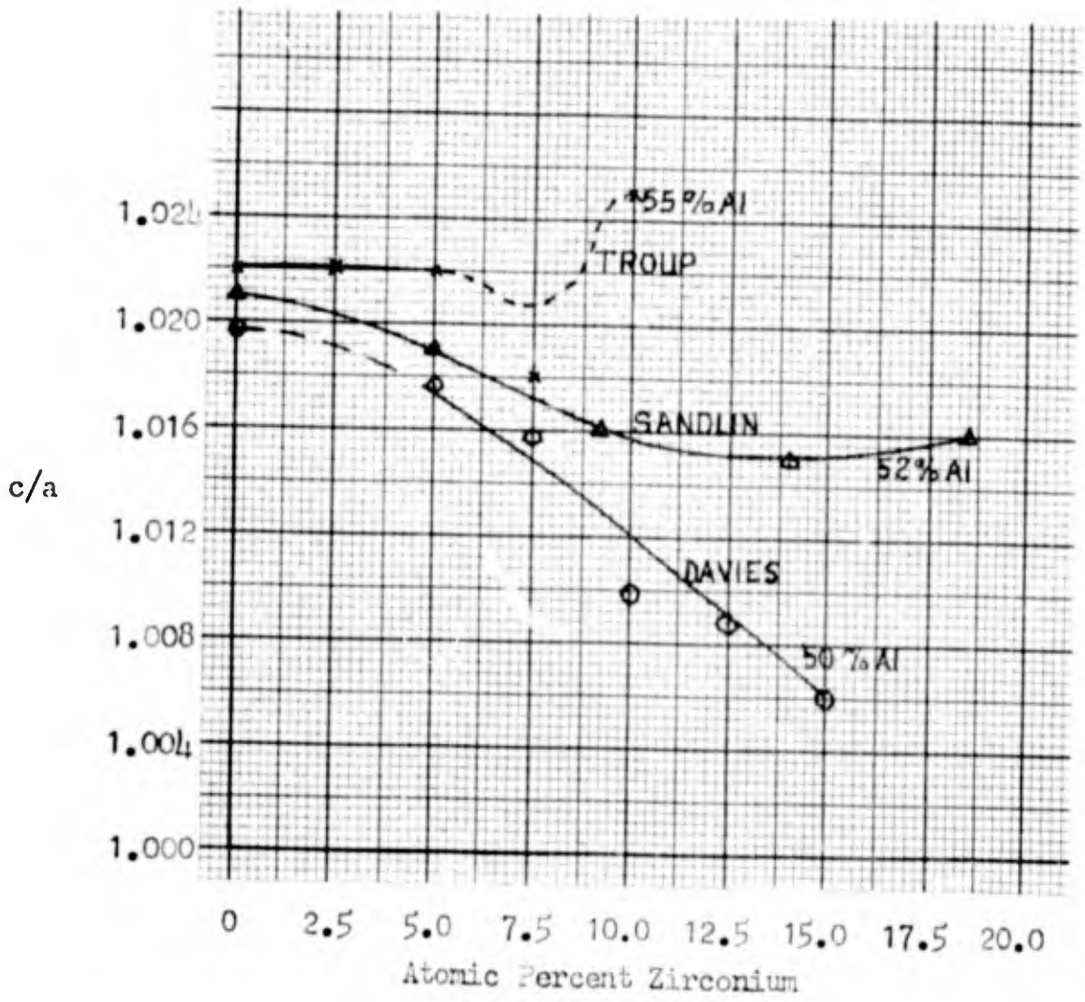

Fig. 4

Variation of c/a Ratio with Zirconium in the Gamma Phase as Determined by Davies, Sandlin, and Troup

There is close agreement in the lattice parameters of binary compositions but there the agreement ends. Both Sandlin and Davies reported decreasing c/a ratios with increasing zirconium content through the gamma phase. However, the results of this investigation indicate a slight decrease and then an increase. In addition, the values of c and a herein reported are slightly lower than those found previously. A possible explanation of the difference lies in the variation in composition between the specimens used in the three examinations and in the difference in their preparation.

TABLE IV

Gamma Phase Lattice Parameters

Specimen No.	Composition (atomic %)			Lattice Parameters (A°)		
	Al	Ti	Zr	c	a	c/a
8	41.96	58.04	-	4.079	3.990	1.002
9	54.74	42.70	2.56	4.085	3.996	1.022
10	55.15	39.90	4.95	4.099	4.011	1.022
11	54.54	37.97	7.49	4.099	4.027	1.018
12	55.11	34.95	9.94	4.132	4.031	1.025
13	46.06	53.94	-	4.054	3.990	1.016
14	59.66	35.39	4.95	4.114	3.990	1.031
15	59.32	30.66	10.01	4.147	4.018	1.032

Sandlin's specimens were air cooled after the homogenizing heat treatment at 2000°F for 36 hours. This slow cooling could allow a change in crystal structure. An examination of diffraction

pattern accompanying Davies' report (Ref 4, Fig. 4) reveals the following unidentified peaks: 1) a moderate reflection at 41°, and 2) weak reflections at 71.5°, 104°, and 145.3°. This could indicate a second phase is present although it is difficult to say without the original diffraction pattern and, with no more than one scan of the dubious areas, an interpretation cannot be made. As Davies' homogenizing treatment was undertaken in an atmosphere of air, rapid contamination of the specimen by oxygen would take place.

Metallographic Analysis

The metallographic investigation of the alloys was disappointing in that the specimens containing 60a/o and higher aluminum content developed microscopic cracks that interferred with phase determination. In addition, as mentioned in Section III, the surfaces became pitted and a smooth surface was unobtainable with manual polishing.

The photograph of specimen 16 (Fig. 22) shows the cracked microstructure. Because of the unfavorable surfaces, the photographs of specimens 13 through 19 were taken in the as-melted condition; that is, of portions of the specimens that were not homogenized. Consequently these photographs were not used in the phase determination.

All specimens were etched with Kroll's etch (3% HF, 6% HNO_3, 91% H_2O). All photomicrographs contained in Appendix G were taken at the University of Dayton Research Institute, Dayton, Ohio

except Fig. 22 which was taken at the Air Force Institute of Technology, Wright-Patterson AFB, Ohio.

The photomicrographs of specimens one through twelve generally support the phase determination by x-ray diffraction. One can observe in specimen 12 (35a/o Ti, 55a/o Al, 10a/o Zr) the precipitation of a second phase. Representative photomicrographs are contained in Appendix G.

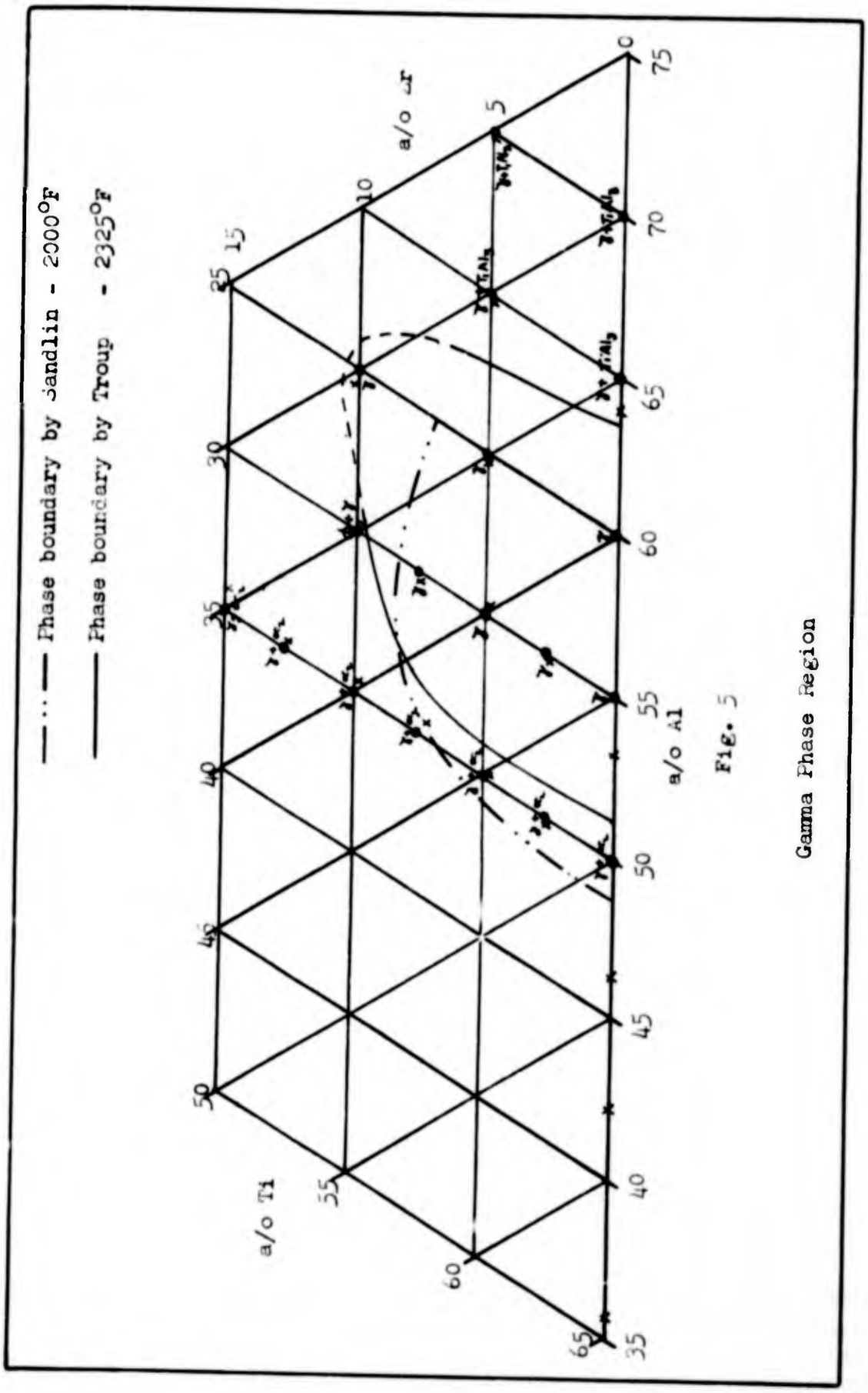

Fig. 5

Gamma Phase Region

IV. Conclusions and Recommendations

1. The solubility of zirconium in the gamma phase increases with temperature. At 2325°F (the average temperature of heat treatment of the specimens in the gamma phase) this phase extends to between 10 and 15a/o zirconium with an aluminum content of 60a/o. At 2000°F and an aluminum content of 58a/o, the limit of solubility is less than 9a/o as reported by Sandlin and shown in Fig. 5.

2. The lower limit of the gamma phase in the Ti-Al binary system is between 50 and 55a/o Al; whereas the upper limit is between 60 and 65a/o Al.

3. The c/a ratio cannot be reduced to unity in this phase through zirconium additions.

The following areas are recommended for further investigation:

1. The gamma phase boundary should be more accurately determined by preparing specimens with a variation in ternary composition of one or two atomic percent.

2. The gamma phase boundary should also be determined at other temperatures both higher and lower.

3. X-ray diffraction should be performed at high temperature (about 2000°F) as well as at room temperature to determine that the c/a ratio does not vary with temperature.

Bibliography

1. Barrett, C. S. Structure of Metals. N. Y.: McGraw-Hill Book Co., Inc., 1952.

2. Buchheit, R. D., et al. Procedure for the Metallographic Preparation of Beryllium, Titanium, and Refractory Metals. DMIC Memorandum 37. Columbus, Ohio: Defense Metals Information Center, Battelle Memorial Institute, October 26, 1959.

3. Cullity, B. D. Elements of X-Ray Diffraction. Reading, Mass.: Addison Wesley, Inc., 1956.

4. Davies, Franklin C. The Effects of Ternary Additions on Lattice Parameters in the Gamma Phase of Titanium-Aluminum Alloy Systems. Unpublished Thesis, Institute of Technology (Air University), Wright-Patterson Air Force Base, Ohio September 1959.

5. De Lella, Amelia. Five Place Table of Natural Trigonometric Functions to Hundredths of a Degree. N. Y.: John Wiley and Sons, Inc., 1934.

6. Duwez, P., and J. L. Taylor. "Crystal Structure of Ti-Al." Journal of Metals, 4:70-71(1952).

7. Ence, Elmars, and H. Margolin. "Phase Relations in the Titanium-Aluminum System." Transactions of the Metallurgical Society of AIME. 221:151-157(February 1961).

8. Goldak, A. J., and H. Gordan Parr. "The Structure of Ti_3Al." Transactions of the Metallurgical Society of AIME. 221:639-640 (June 1961).

9. Kessler, H. D., and J. B. McAndrew. Investigation of the Metallurgical Characteristics of the 36% Aluminum Titanium-Base Alloy. WADC Tech. Report 53-182, July 1953.

10. Maykuth, D. J. et al. The Effects of Alloying Elements in Titanium. Columbus, Ohio: Defense Metals Information Center, Battelle Memorial Institute, September 15, 1960.

11. Myers, Edward J., and Franklin C. Davies. "A Direct Graphical Method for the Precise Determination of Lattice Parameters of Tetragonal or Hexagonal Crystals." Acta Crystallographica. 14:194-197(1961).

12. Rhines, Frederick N. Phase Diagram in Metallurgy. N. Y.: McGraw-Hill Book Company, Inc., 1956.

13. Sandlin, D. R., and H. A. Klung, Jr. A Phase Study of a Selected Portion of the Ti-Al-Zr Ternary System Including Lattice Parameter Determination for the Ti-Al Gamma Phase. Unpublished Thesis, Institute of Technology (Air University), Wright-Patterson Air Force Base, Ohio, August 1961.

14. _____. X-Ray Powder Data File (Eighth Set). Philadelphia: American Society for Testing Materials, 1958.

Appendix A

Tetragonal Crystal Structure of Ti-Al

The tetragonal crystal is a six-sided figure with adjacent sides joined at right angles. The top and base are square and the four sides are rectangular. The height of the crystal is denoted by 'c' and the length of one edge of the base is labelled 'a'. The c/a ratio thus indicates the relationship of the height of the crystal to the base. This ratio also shows the departure of the crystal from a cubic structure as a c/a ratio of unity applies to the special case of a cube.

In the simple tetragonal crystal there is an atom at each corner and each atom is shared by the eight cells that meet at the corner. This results in one atom per unit cell. In the face-centered crystal there is an atom in the center of the six sides. Each of these atoms is shared by two cells so the face-centered cell has three more atoms than the simple cell. Therefore, each primary face-centered tetragonal crystal has a total of four atoms.

In the case of the ordered-face-centered crystal such as Ti-Al, the layer of atoms at the base of the crystal is composed of one element and the next layer is made up of atoms of the other element. This structure is shown in Fig. 6. When zirconium is substituted for titanium the atoms in the Ti layer are replaced whereas the aluminum atoms remain as before.

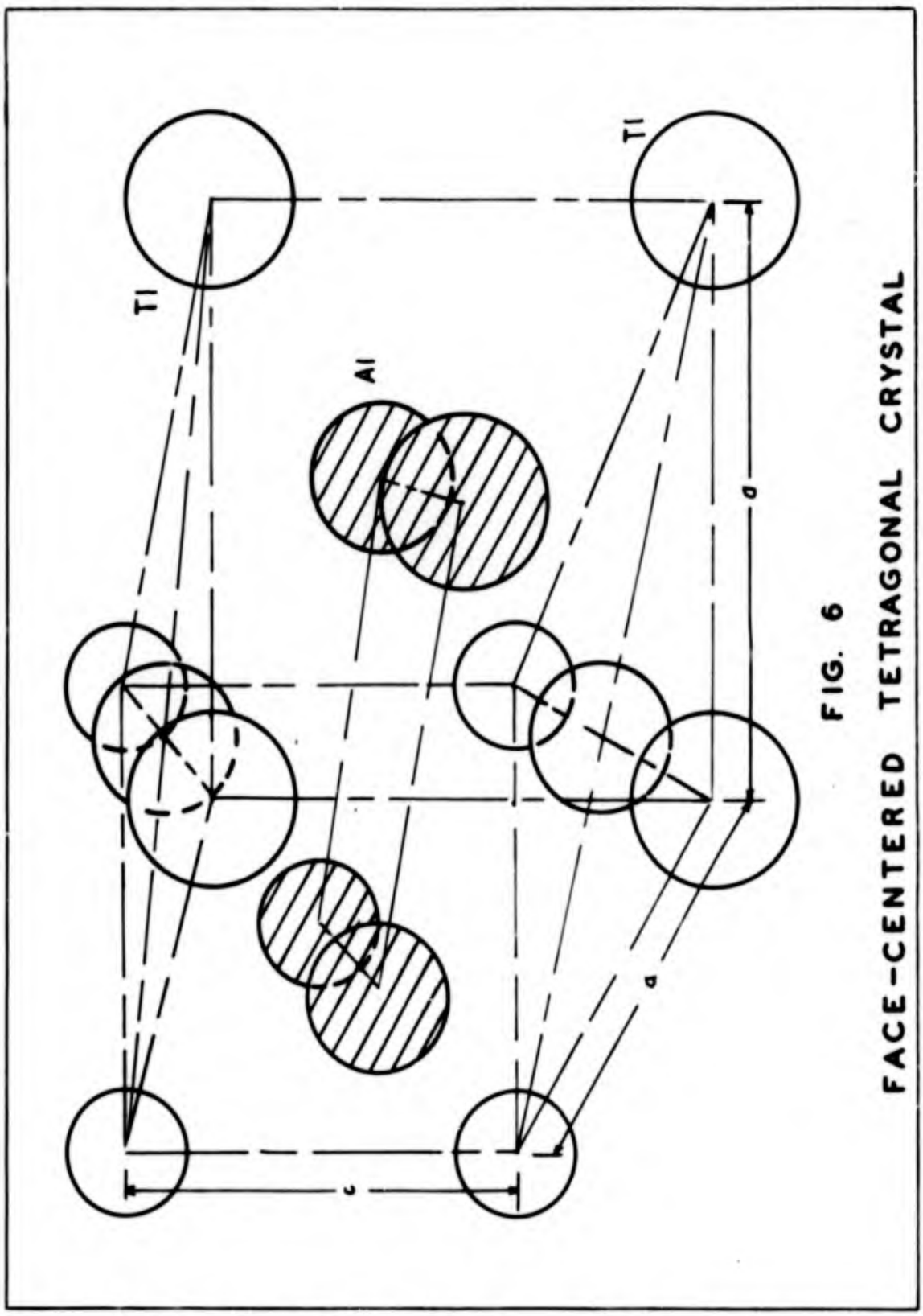

FIG. 6

FACE-CENTERED TETRAGONAL CRYSTAL

Appendix B

Chemical Analyses

As approximately one gram was lost from each sample during the melting operation, a chemical analysis was deemed desirable. If the weight loss were composed primarily of aluminum (a possibility due to its lower melting point), the actual composition would differ from the nominal composition by as much as five percent. Spectrographic analyses were made and the results indicated the aluminum to be in error by 10 to 20 weight percent. In two cases the aluminum percentage content increased and in the others the aluminum content decreased with respect to the nominal composition. This much change in content was unaccountable so wet chemical analyses were made.

In the case of the ternary alloys the results of the wet chemical analyses agreed with the nominal values within one percent. However, there was disagreement in the case of the binary alloys and the difference was too great to be accounted for by weight loss. The diffraction patterns of the binary alloys indicate the same phases as are present in the ternary alloys containing the same nominal amount of aluminum. Consequently, the nominal content was used throughout. The results of the chemical analyses are indicated in Fig. 7.

The analyses were performed by the Bowser-Morner Testing Laboratories, Inc., Dayton, Ohio. The atomic percent content was computed from the weight percent content.

The nominal content and the results of the chemical analyses are listed in the following tables:

TABLE V

Nominal Composition

Note: All values are in atomic percent

Specimen	Aluminum	Titanium	Zirconium
1	50.00	50.00	-
2	50.00	47.50	2.50
3	50.00	45.00	5.00
4	50.00	42.50	7.50
5	50.00	40.00	10.00
6	50.00	37.50	12.50
7	50.00	35.00	15.00
8	55.00	45.00	-
9	55.00	42.50	2.50
10	55.00	40.00	5.00
11	55.00	37.50	7.50
12	55.00	35.00	10.00
13	60.00	40.00	-
14	60.00	35.00	5.00
15	60.00	30.00	10.00
16	65.00	35.00	-
17	65.00	30.00	5.00
18	70.00	30.00	-
19	70.00	25.00	5.00

TABLE VI

Nominal Composition

Note: All values are in weight percent

Specimen	Aluminum	Titanium	Zirconium
1	36.00	64.00	-
2	35.01	59.07	5.92
3	34.05	54.43	11.52
4	33.14	50.04	16.82
5	32.28	45.87	21.84
6	31.57	41.92	26.61
7	30.70	38.16	31.14
8	40.76	59.24	-
9	39.59	54.33	6.09
10	38.47	49.70	11.83
11	37.42	45.32	17.26
12	36.43	41.17	22.40
13	45.79	54.21	-
14	43.14	44.70	12.16
15	40.79	36.22	22.99
16	51.12	48.88	-
17	48.08	39.41	12.51
18	56.78	43.22	-
19	53.31	33.81	12.88

TABLE VII

Chemical Analysis

Note: All values are in atomic percent

Specimen	Aluminum	Titanium	Zirconium
1	35.68	64.32	-
2	49.58	47.99	2.41
3	50.10	45.12	4.79
4	50.55	42.45	6.99
5	50.33	39.95	9.72
6	50.21	37.37	12.42
7	50.26	34.40	14.98
8	41.96	58.04	-
9	54.74	42.70	2.56
10	55.15	39.90	4.95
11	54.54	37.97	7.49
12	55.11	34.95	9.94
13	46.06	53.94	-
14	59.66	35.39	4.95
15	59.32	30.66	10.01
16	53.18	46.82	-
17	64.73	30.29	4.98
18	63.97	36.03	-
19	69.92	25.14	4.94

TABLE VIII

Wet Chemical Analysis

Note: All values are in weight percent

Specimen	Aluminum	Titanium	Zirconium
1	23.70	75.85	-
2	34.62	59.49	5.70
3	34.16	54.63	11.04
4	33.70	50.24	15.76
5	32.56	45.89	21.28
6	31.60	41.75	26.43
7	31.11	37.53	31.13
8	28.86	70.88	-
9	39.15	54.22	6.17
10	38.60	49.57	11.72
11	36.97	45.68	17.17
12	36.50	41.09	22.25
13	32.40	67.36	-
14	42.74	45.01	11.99
15	40.15	36.84	22.91
16	38.93	60.84	-
17	47.69	39.61	12.40
18	49.80	49.80	-
19	53.20	33.95	12.73

By Bowser-Morner Testing Lab., Inc.

TABLE IX

Spectrographic Analysis

Note: All values are in weight percent

Specimen	Aluminum	Titanium	Zirconium
1	25.31	74.12	-
2	23.08	66.40	10.02
3	25.28	54.28	20.06
4	20.88	51.02	28.08
5	15.92	49.24	34.21
6	16.04	43.40	40.10
7	15.30	36.60	47.40
8	27.80	71.48	-
9	25.60	63.50	10.25
10	25.12	56.04	18.30
11	23.48	47.90	28.10
12	18.60	38.40	42.26
13	32.44	66.82	-
14	29.92	49.38	20.80
15	21.60	34.16	43.70
16	36.68	62.50	-
17	51.91	38.86	9.23
18	42.20	57.18	-
19	37.48	41.60	20.72

By Bowser-Morner Testing Lab., Inc.

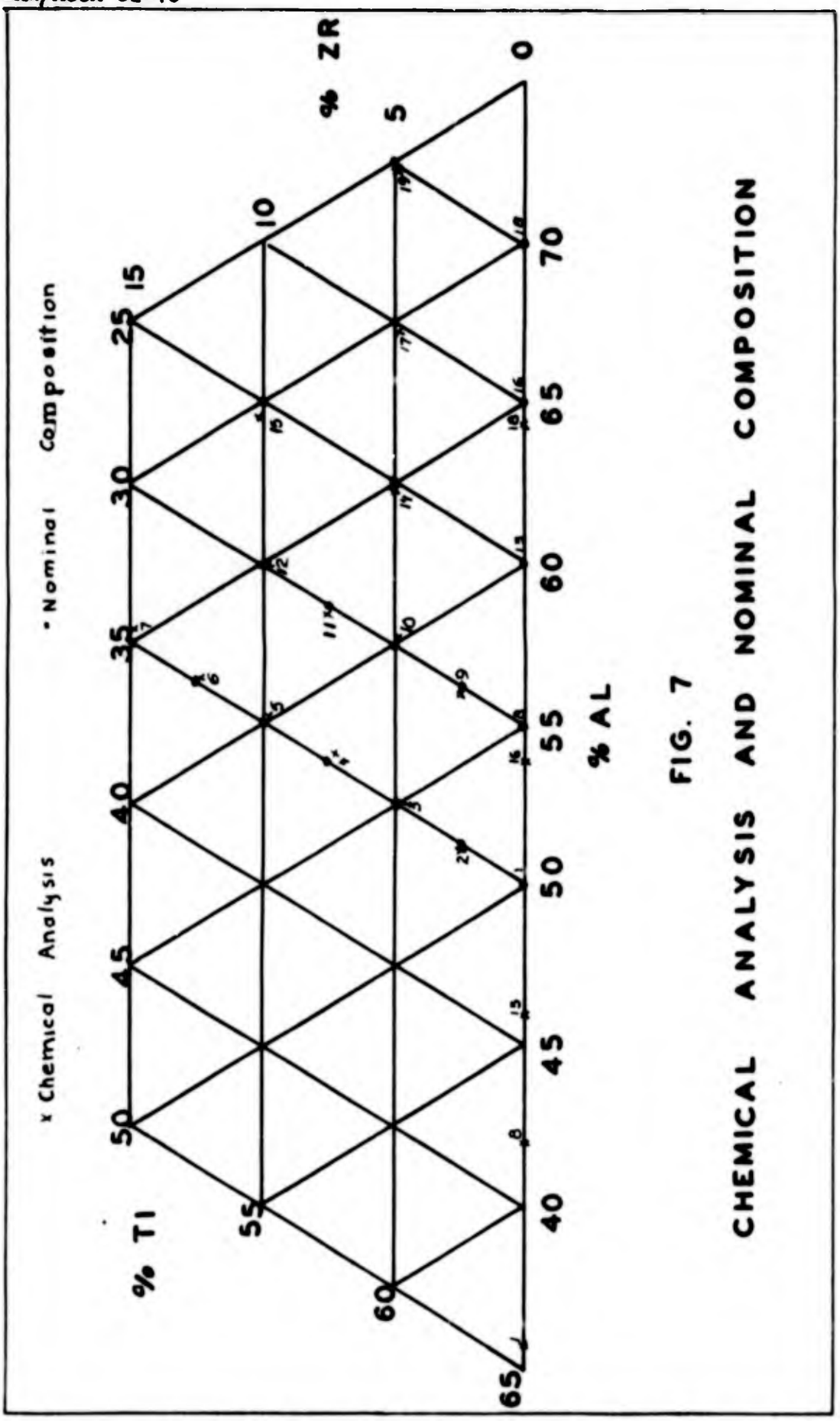

FIG. 7

CHEMICAL ANALYSIS AND NOMINAL COMPOSITION

Appendix C

Graphs of Reflecting Planes of the Gamma Phase

The variation in location of 2θ (to 84°) of the gamma phase with changes in composition is shown in the accompanying figures. In general, the 2θ values decrease with an increase in zirconium and increase slightly with an increase in aluminum.

The failure of the crystal to attain the cubic structure is indicated in reflections of planes like (200), (002), (113), and (131). The (200) and (002) planes and the (113) and (131) planes would coincide in a cubic crystal but they remain separate throughout the gamma phase.

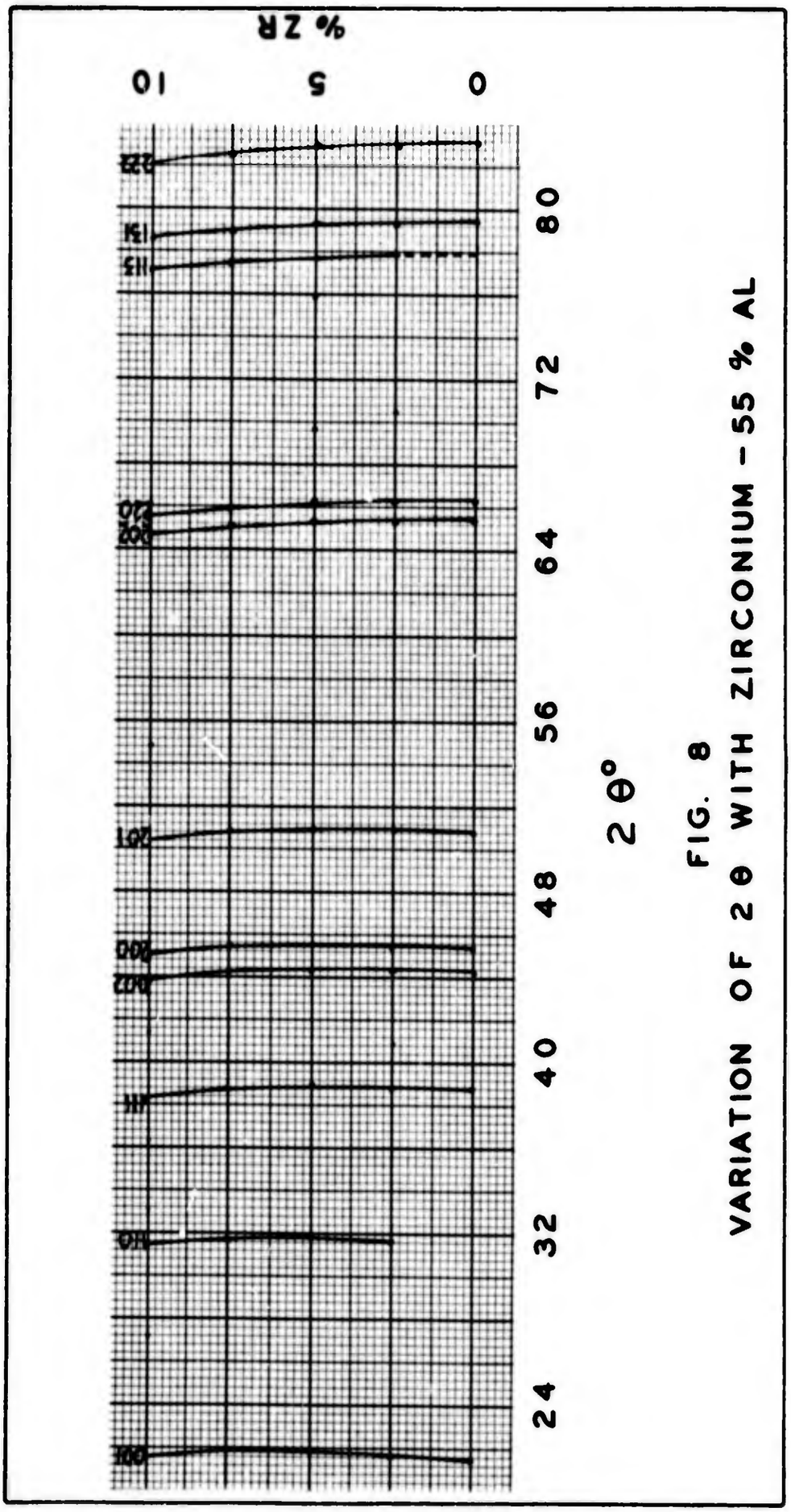

FIG. 8
VARIATION OF 2θ WITH ZIRCONIUM - 55 % AL

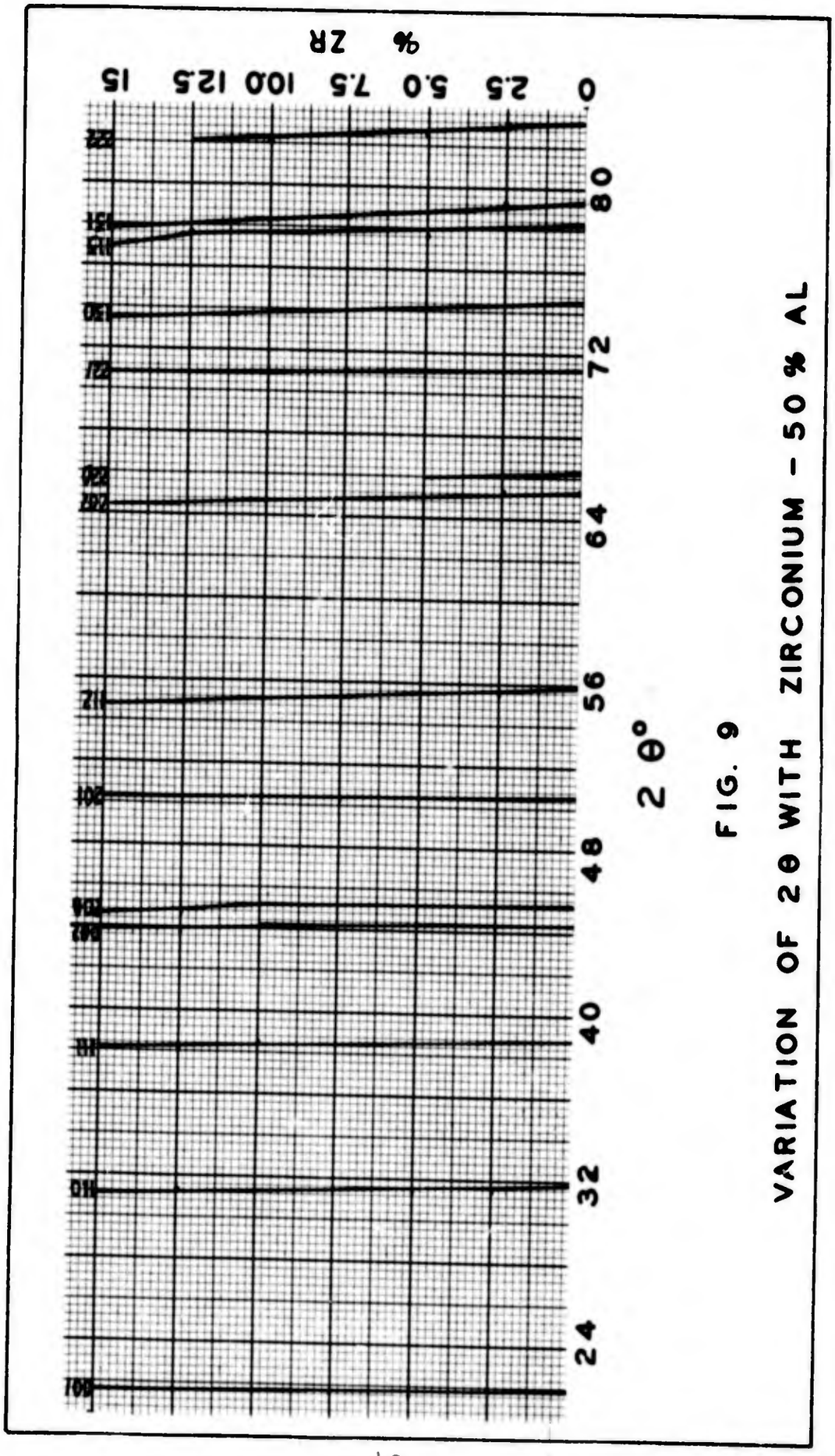

FIG. 9

VARIATION OF 2θ WITH ZIRCONIUM - 50 % AL

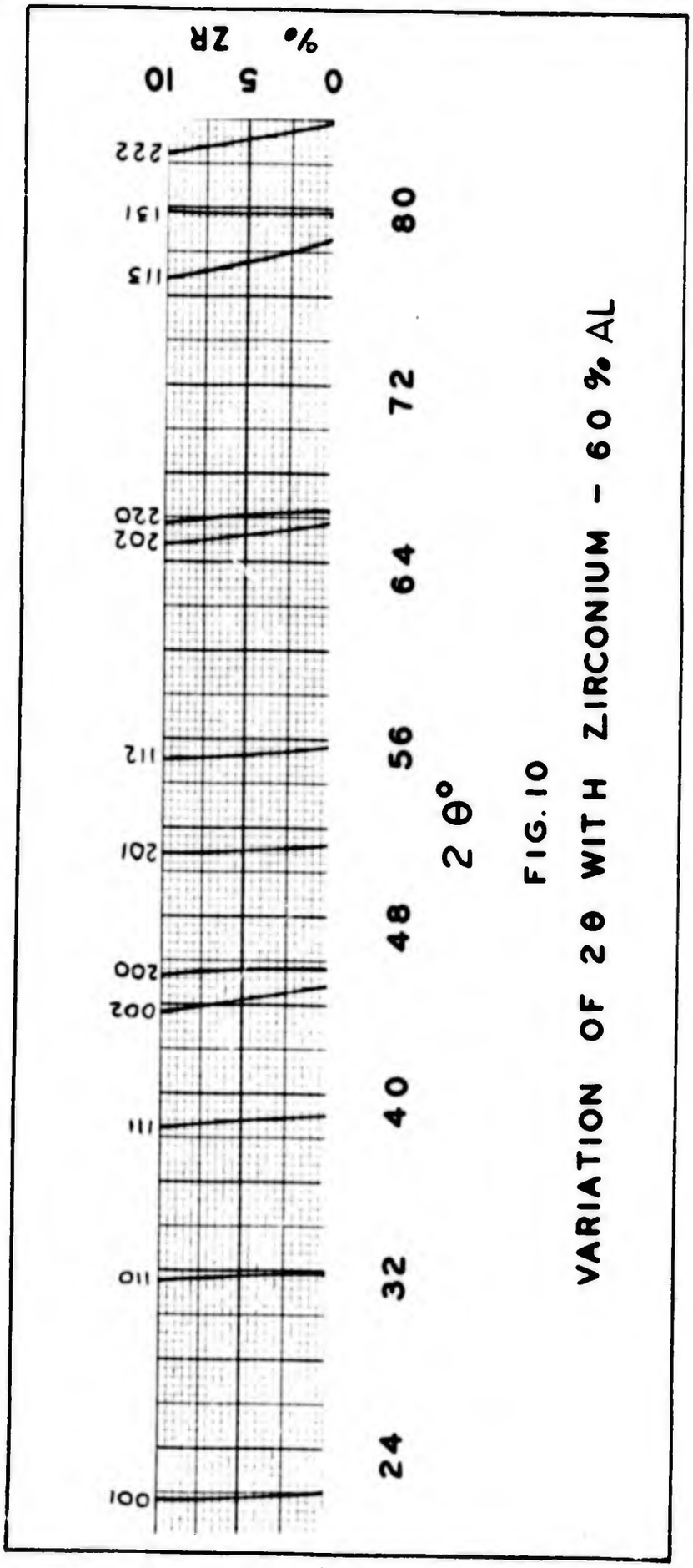

FIG. 10

VARIATION OF 2θ WITH ZIRCONIUM - 60 % AL

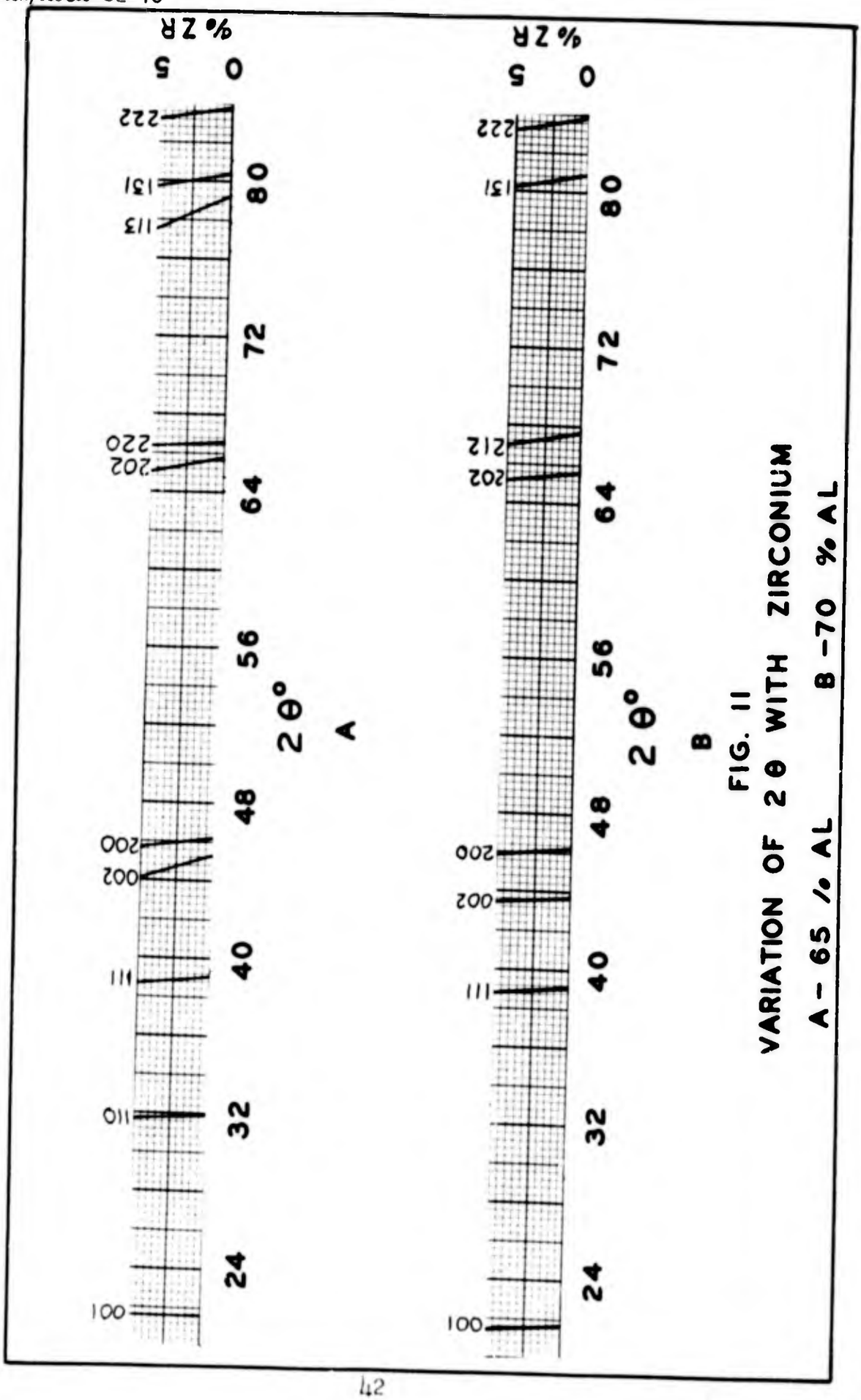

FIG. 11
VARIATION OF 2θ WITH ZIRCONIUM
A – 65 % AL B –70 % AL

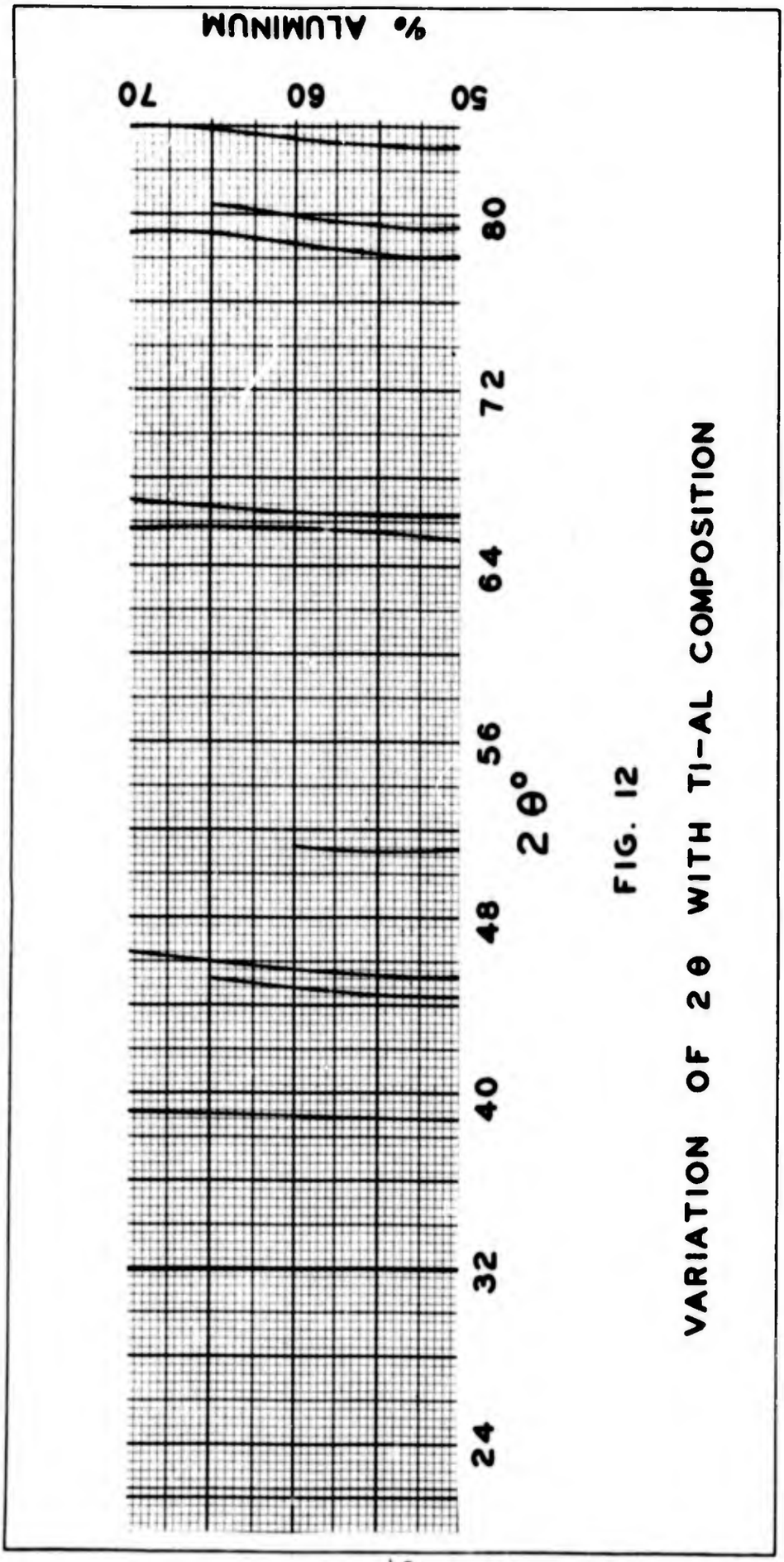

FIG. 12

VARIATION OF 2θ WITH TI-AL COMPOSITION

VARIATION OF 2θ WITH ALUMINUM – 5% ZR

FIG. 13

Appendix D

Tabulation of 2θ Values with Intensities and Identities

The determination of 2θ values was mentioned in Section III and the accompanying tables contain a list of the peaks with their 2θ values.

The relative intensities are indicated by:

VVS - very, very strong

VS - very strong

S - strong

M - moderate

W - weak

VW - very weak

VVW - very, very weak

TABLE X

2θ Angles, Intensities, and Identities of Peaks

Specimen 1 (Ti 50a/o, Al 50a/o)

Peak No.	2θ Value Degrees	Intensity	Identity
1	21.8	M	γ(001)
2	32.0	W	γ(110)
3	36.5	VW	α_2(400)
4	38.8	VS	γ(111)
5	41.4	W	α_2(401)
6	44.6	M	γ(002)
7	45.4	S	γ(200)
8	50.3	VW	γ(102)
9	51.1	W	γ(210)
10	54.2	W	α_2(402)
11	55.8	W	γ(112)
12	62.9	VW	γ(203)
13	64.3	VW	α_2(440)
14	65.3	M	γ(202)
15	66.3	W	γ(220)
16	69.8	VW	γ(003)
17	72.1	VW	α_2(403)
18	76.2	VW	α_2(800)
19	78.2	W	γ(113)
20	79.3	M	γ(131)
21	83.2	W	γ(222)
22	88.7	W	α_2(802)
23	94.2	W	α_2(404)
24	98.7	M	γ(004)
25	101.0	W	γ(400)
26	112.4	M	γ(313)
27	116.5	S	γ(204)
28	118.2	M	γ(402)
29	120.3	W	γ(420)
30	124.7	W	γ(421)
31	128.9	W	γ(332)
32	135.0	W	α_2(425)
33	137.4	M	γ(224)
34	140.6	W	γ(422)

BLANK PAGE

TABLE XI

2θ Angles, Intensities, and Identities of Peaks

Specimen 2 (Ti 47.5a/o. Al 50a/o, Zr 2.5a/o)

Peak No.	2θ Value Degrees	Intensity	Identity
1	21.9	M	γ(001)
2	26.5	VW	α_4(201)
3	31.5	W	γ(110)
4	38.7	VS	γ(111)
5	41.0	M	α_4(401)
6	44.3	W	γ(002)
7	45.3	M	γ(200)
8	50.3	W	γ(201)
9	53.9	W	α_2(402)
10	55.5	VW	γ(112)
11	65.3	M	γ(202)
12	70.2	W	γ(221)
13	72.3	W	α_2(403)
14	75.8	W	γ(130)
15	78.1	W	γ(113)
16	79.3	M	γ(131)
17	81.7	W	-
18	83.2	M	γ(222)
19	89.6	W	α_2(802)
20	92.0	W	γ(132)
21	94.3	W	α_1(404)
22	98.3	W	γ(004)
23	105.1	W	γ(401)
24	110.4	VW	γ(330)
25	112.8	M	γ(313)
26	118.5	W	γ(402)
27	119.2	W	γ(420)
28	123.7	W	α_1(405)
29	125.6	M	-
30	137.2	M	γ(224)
31	140.9	M	γ(422)
32	145.8	W	γ(403)
33	148.0	W	-
34	149.3	W	γ(105)
35	157.6	W	γ(501)

TABLE XII

2θ Angles, Intensities, and Identities of Peaks

Specimen 3 (Ti 45a/o, Al 50a/o, Zr 5a/o)

Peak No.	2θ Value Degrees	Intensity	Identity
1	21.5	M	γ(001)
2	27.0	W	α_1(201)
3	31.4	W	γ(110)
4	38.6	VS	δ(111)
5	40.9	M	α_2(401)
6	44.2	M	γ(002)
7	45.1	M	δ(200)
8	50.5	W	γ(201)
9	65.0	M	γ(202)
10	65.9	W	γ(220)
11	77.6	M	δ(113)
12	78.8	S	γ(131)-α_2(442)
13	82.6	M	δ(222)
14	86.1	W	δ(203)
15	88.6	W	α_1(802)
16	96.2	VW	-
17	97.7	W	δ(004)
18	103.4	W	δ(223)
19	105.1	W	δ(401)
20	111.7	M	α_2(841)
21	113.0	W	γ(313)
22	114.8	W	γ(331)
23	117.3	M	α_2(402)
24	119.8	W	γ(420)
25	129.6	W	α_1(804)
26	137.3	W	γ(224)
27	138.6	M	-
28	139.1	W	-
29	156.9	W	α_2(1202)

TABLE XIII

2θ Angles, Intensities, and Identities of Peaks

Specimen 4 (Ti 42.5a/o, Al 50a/o, Zr 7.5a/o)

Peak No.	2θ Value Degrees	Intensity	Identity
1	21.6	M	γ(001)
2	25.2	W	-
3	31.5	W	γ(110)
4	36.8	W	α_2(400)
5	38.5	VVS	γ(111)
6	40.7	M	α_2(401)
7	44.2	M	γ(002)
8	45.1	M	γ(200)
9	50.3	W	γ(102)
10	54.6	W	α_2(402)
11	64.9	M	γ(202)
12	71.1	W	γ(221)
13	77.4	M	α_2(801)
14	78.4	M	γ(131)-α_2(442)
15	87.0	W	γ(203)
16	99.4	W	-
17	111.0	M	γ(330)
18	115.0	W	γ(331)
19	116.8	M	α_2(444)- γ(204)
20	123.7	VW	γ(421)
21	125.9	VVW	-
22	129.4	W	α_2(804)
23	132.3	VW	-
24	135.4	W	α_2(425)
25	137.8	W	γ(224)
26	142.6	VW	γ(005)
27	148.7	W	-
28	151.6	W	-

TABLE XIV

2θ Angles, Intensities, and Identities of Peaks

Specimen 5 (Ti 40a/o, Al 50a/o, Zr 10a/o)

Peak No.	2θ Value Degrees	Intensity	Identity
1	21.7	M	γ(001)
2	29.4	VW	-
3	31.4	W	γ(110)
4	34.5	VW	-
5	35.5	VW	-
6	36.5	W	α_2(400)
7	38.5	VVS	γ(111)
8	40.9	M	α_2(401)
9	44.2	M	γ(002)
10	45.2	W	γ(200)
11	50.4	M	γ(201)
12	53.6	W	α_2(402)
13	57.9	W	-
14	64.6	S	γ(202)
15	71.2	W	α_2(403)
16	73.9	W	γ(301)
17	75.6	W	α_2(800)
18	77.6	M	γ(113)
19	78.2	S	γ(131) - α_2(442)
20	82.0	M	γ(222)
21	90.5	W	γ(132)
22	94.8	W	-
23	97.7	W	-
24	98.7	W	γ(400)
25	102.2	W	α_2(803)
26	111.2	M	γ(331)
27	116.4	M	γ(420)
28	128.1	W	-
29	130.0	W	-
30	135.5	W	-
31	136.8	M	γ(422)
32	140.7	W	α_2(843)
33	147.0	W	-
34	153.2	W	γ(115)

TABLE XV

2θ Angles, Intensities, and Identities of Peaks

Specimen 6 (Ti 37.5a/o, Al 50a/o, Zr 12.5a/o)

Peak No.	2θ Value Degrees	Intensity	Identity
1	21.6	M	δ(001)
2	31.4	W	γ(110)
3	35.5	W	-
4	36.7	W	α_2(400)
5	38.2	VS	γ(111)
6	41.5	W	α_2(401)
7	43.8	W	γ(002)
8	44.5	M	γ(200)
9	47.1	VW	α_2(420)
10	54.8	VW	γ(112)
11	64.4	M	γ(202)
12	77.7	W	γ(113)
13	82.1	W	γ(222)
14	98.2	W	γ(400)
15	101.0	W	α_2(803)
16	104.0	VW	γ(114)
17	106.3	W	α_2(840)
18	110.4	M	γ(331)
19	115.7	M	γ(420)
20	130.0	W	α_2(425)
21	135.7	W	γ(422)
22	143.2	VW	-
23	151.2	W	γ(115)

TABLE XVI

2θ Angles, Intensities, and Identities of Peaks

Specimen 7 (Ti 35a/o, Al 50a/o, Zr 15a/o)

Peak No.	2θ Value Degrees	Intensity	Identity
1	21.6	M	γ(001)
2	31.0	W	γ(110)
3	32.8	W	-
4	36.4	W	α_2(400)
5	38.2	VS	γ(111)
6	40.4	W	α_2(401)
7	44.0	M	γ(002)
8	44.6	S	γ(200)
9	50.2	W	γ(102)
10	52.4	VW	-
11	64.4	M	γ(202)
12	70.8	W	γ(221)
13	72.5	W	γ(103)
14	77.0	M	γ(113)
15	77.8	M	α_2(442)- γ(131)
16	82.9	W	-
17	90.2	W	γ(132)
18	92.2	W	α_2(404)
19	93.4	W	-
20	96.0	W	γ(004)
21	97.2	W	γ(400)
22	105.8	W	α_2(840)
23	110.4	M	γ(331)
24	115.0	M	γ(420)
25	134.1	W	γ(422)
26	135.9	W	γ(005)

TABLE XVII

2θ Angles, Intensities, and Identities of Peaks

Specimen 8 (Ti 45a/o, Al 55a/o)

Peak No.	2θ Value Degrees	Intensity	Identity
1	21.4	M	γ(001)
2	38.8	VS	γ(111)
3	44.3	W	γ(002)
4	45.4	M	γ(200)
5	50.8	VW	γ(201)
6	65.4	M	γ(202)
7	66.3	W	γ(220)
8	78.0	W	γ(113)
9	79.5	M	γ(131)
10	83.1	W	γ(222)
11	92.2	W	γ(132)
12	98.3	W	γ(004)
13	101.1	W	γ(400)
14	107.0	VW	γ(114)
15	112.8	M	γ(313)
16	114.3	W	γ(331)
17	116.1	W	γ(204)
18	119.1	M	γ(402)
19	137.4	M	γ(224)
20	141.0	M	γ(422)
21	146.4	W	γ(403)

TABLE XVIII

2θ Angles, Intensities, and Identities of Peaks

Specimen 9 (Ti 42.5a/o, Al 55a/o, Zr 2.5a/o)

Peak No.	2θ Value Degrees	Intensity	Identity
1	21.6	M	γ(001)
2	31.6	W	γ(110)
3	38.8	VS	γ(111)
4	40.9	W	-
5	44.3	M	γ(002)
6	45.4	S	γ(200)
7	51.0	W	γ(201)
8	65.3	S	γ(202)
9	66.2	W	γ(220)
10	70.5	VW	γ(221)
11	77.7	M	γ(113)
12	79.3	M	γ(131)
13	83.0	M	γ(222)
14	86.3	W	γ(203)
15	88.8	W	γ(213)
16	92.0	VW	γ(132)
17	97.8	W	γ(004)
18	101.0	W	γ(400)
19	103.5	W	γ(223)
20	104.9	W	γ(401)
21	112.4	M	γ(313)
22	114.2	W	γ(331)
23	116.2	W	γ(204)
24	118.6	M	γ(402)
25	137.0	M	γ(224)
26	140.8	W	γ(422)
27	146.4	W	γ(403)

TABLE XIX

2θ Angles, Intensities, and Identities of Peaks

Specimen 10 (Ti 40a/o, Al 55a/o, Zr 5a/o)

Peak No.	2θ Value Degrees	Intensity	Identity
1	21.9	M	δ(001)
2	32.0	W	γ(110)
3	39.0	VS	δ(111)
4	44.4	M	γ(002)
5	45.6	S	δ(200)
6	51.0	W	δ(201)
7	65.5	M	γ(202)
8	66.2	W	δ(220)
9	69.6	VW	δ(003)
10	75.9	W	γ(130)
11	77.6	M	γ(113)
12	79.3	S	γ(131)
13	82.9	M	δ(222)
14	91.2	W	δ(213)
15	97.8	W	δ(004)
16	100.6	W	γ(400)
17	112.1	M	γ(313)
18	114.9	W	-
19	118.7	M	γ(402)
20	136.0	W	γ(224)
21	139.4	W	γ(422)

TABLE XX

2θ Angles, Intensities, and Identities of Peaks

Specimen 11 (Ti 37.5a/o, Al 55a/o, Zr 7.5a/o)

Peak No.	2θ Value Degrees	Intensity	Identity
1	21.9	M	γ(001)
2	31.7	W	γ(110)
3	38.7	VS	γ(111)
4	44.2	W	γ(002)
5	45.5	M	γ(200)
6	50.9	VW	γ(201)
7	65.1	M	γ(202)
8	65.8	W	γ(220)
9	68.3	W	γ(212)
10	77.4	M	γ(113)
11	78.8	S	γ(131)
12	82.4	S	γ(222)
13	88.7	W	γ(213)
14	90.8	W	γ(132)
15	94.2	W	-
16	98.2	W	γ(004)
17	102.7	VW	γ(223)
18	111.6	M	γ(313)
19	112.6	W	γ(331)
20	116.2	W	γ(204)
21	117.4	M	γ(402)
22	135.3	W	γ(224)
23	138.2	W	γ(422)
24	153.4	W	γ(510)

TABLE XXI

2θ Angles, Intensities, and Identities of Peaks

Specimen 12 (Ti 35a/c, Al 55a/c, Zr 10a/c)

Peak No.	2θ Value Degrees	Intensity	Identity
1	21.6	M	γ (001)
2	27.6	VW	ø
3	31.4	W	γ (110)
4	33.1	VVW	ø
5	36.3	VW	ø
6	38.4	VS	γ (111)
7	41.4	VW	ø
8	42.6	VW	ø
9	43.9	M	γ (002)
10	45.0	S	γ (200)
11	50.4	W	γ (201)
12	54.8	W	γ (112)
13	64.7	W	γ (202)
14	65.5	W	γ (220)
15	76.9	W	γ (113)
16	78.6	M	γ (131)
17	82.1	W	γ (222)
18	84.6	VW	ø
19	96.7	W	γ (004)
20	99.0	W	γ (400)
21	110.9	M	γ (313)
22	112.5	W	γ (331)
23	113.8	W	γ (204)
24	116.6	W	γ (420)
25	128.7	VW	ø
26	134.4	W	γ (224)
27	137.2	W	γ (422)
28	152.6	W	γ (510)
29	157.4	W	γ (115)

TABLE XXII

2θ Angles, Intensities, and Identities of Peaks

Specimen 13 (Ti 40a/o, Al 60a/o)

Peak No.	2θ Value Degrees	Intensity	Identity
1	22.0	W	γ(001)
2	31.9	W	γ(110)
3	36.0	W	-
4	39.0	VS	γ(111)
5	44.9	S	γ(002)
6	45.6	S	γ(200)
7	50.3	VW	δ(102)
8	51.2	W	γ(201)
9	55.7	W	γ(112)
10	65.8	S	γ(202)
11	66.2	W	γ(220)
12	68.7	VW	γ(212)
13	69.7	VW	γ(003)
14	73.2	W	γ(103)
15	78.6	M	δ(113)
16	79.6	M	δ(131)
17	83.8	W	δ(222)
18	89.4	VW	γ(213)
19	98.2	W	δ(004)
20	101.05	W	γ(400)
21	107.0	W	δ(114)
22	110.7	W	δ(330)
23	113.4	M	γ(313)
24	117.5	W	δ(204)
25	118.8	M	γ(402)
26	138.8	W	δ(224)
27	141.2	M	δ(422)
28	153.7	W	γ(314)

TABLE XXIII

2θ Angles, Intensities, and Identities of Peaks

Specimen 14 (Ti 35a/o, Al 60a/o, Zr 5a/o)

Peak No.	2θ Value Degrees	Intensity	Identity
1	21.6	M	β(001)
2	29.6	VW	-
3	31.9	W	γ(110)
4	38.9	VS	β(111)
5	44.2	M	β(002)
6	45.6	S	γ(200)
7	50.8	W	γ(201)
8	55.3	W	γ(112)
9	65.2	M	γ(202)
10	66.2	W	γ(220)
11	70.4	W	γ(221)
12	77.4	M	β(113)
13	79.5	S	γ(131)
14	83.0	M	β(222)
15	86.6	W	γ(203)
16	91.2	W	γ(132)
17	97.1	W	β(004)
18	101.1	M	γ(400)
19	109.8	VW	γ(330)
20	112.1	M	β(313)
21	114.6	M	γ(331)
22	116.3	VW	γ(204)
23	118.3	M	γ(402)
24	124.0	W	γ(421)
25	129.4	VW	γ(332)
26	135.8	W	γ(224)
27	140.4	M	γ(422)
28	146.3	W	γ(403)
29	154.3	W	β(115)
30	156.3	VW	β(510)

TABLE XXIV

2θ Angles, Intensities, and Identities of Peaks

Specimen 15 (Ti 30a/o, Al 60a/o, Zr 10a/o)

Peak No.	2θ Value Degrees	Intensity	Identity
1	21.6	M	γ(001)
2	27.3	W	-
3	31.5	W	γ(110)
4	35.0	VW	-
5	38.4	VS	γ(111)
6	43.7	M	γ(002)
7	45.2	S	γ(200)
8	50.8	W	γ(201)
9	55.0	VW	γ(112)
10	64.7	M	γ(202)
11	65.7	M	γ(220)
12	76.8	W	γ(113)
13	78.9	M	γ(131)
14	82.4	W	γ(222)
15	96.1	W	γ(004)
16	100.3	M	γ(400)
17	111.0	M	γ(313)
18	113.2	M	γ(331)
19	117.5	M	γ(402)
20	123.0	W	γ(421)
21	126.8	VW	γ(332)
22	134.5	W	γ(224)
23	138.3	M	γ(422)
24	143.6	W	γ(403)
25	151.3	W	γ(314)

TABLE XXV

2θ Angles, Intensities, and Identities of Peaks

Specimen 16 (Ti 35a/o, Al 65a/o)

Peak No.	2θ Value Degrees	Intensity	Identity
1	21.6	M	γ(001)
2	31.9	W	γ(110)
3	33.0	W	$TiAl_3$
4	39.1	VS	γ(111)
5	45.3	S	γ(002)
6	46.1	M	γ(200)
7	65.7	M	γ(202)
8	66.5	M	γ(220)
9	69.5	VVW	$TiAl_3$
10	76.5	W	γ(130)
11	79.1	S	γ(113)
12	80.5	M	γ(131)
13	82.6	W	$TiAl_3$
14	83.8	M	γ(222)
15	95.9	VW	-
16	100.3	W	-
17	103.0	W	γ(400)
18	106.0	W	γ(223)
19	113.8	M	γ(313)
20	114.9	M	γ(331)
21	118.2	M	γ(402)
22	120.7	M	$TiAl_3$
23	140.4	M	-
24	143.5	W	γ(422)

TABLE XXVI

2θ Angles, Intensities, and Identities of Peaks

Specimen 17 (Ti 30a/o, Al 65a/o, Zr 5a/o)

Peak No.	2θ Value Degrees	Intensity	Identity
1	21.6	M	γ(001)
2	31.8	W	γ(110)
3	35.0	W	-
4	38.7	VS	γ(111)
5	42.3	W	$TiAl_3$
6	44.0	W	γ(002)
7	45.6	M	γ(200)
8	47.8	W	$TiAl_3$
9	51.2	W	γ(201)
10	54.7	VW	$TiAl_3$
11	63.0	VW	$TiAl_3$
12	65.2	M	γ(202)
13	66.4	W	γ(220)
14	77.3	W	γ(113)
15	79.6	W	γ(131)
16	83.1	W	γ(222)
17	91.6	W	γ(132)
18	93.8	W	$TiAl_3$
19	94.7	W	-
20	96.6	W	-
21	101.7	W	γ(400)
22	105.6	W	γ(401)
23	112.3	M	γ(313)
24	114.8	M	γ(331)
25	116.8	W	γ(224)
26	118.6	W	γ(402)
27	119.9	W	γ(420)
28	123.0	W	$TiAl_3$
29	129.2	W	$TiAl_3$
30	130.1	W	γ(332)
31	135.8	M	-
32	137.3	W	γ(224)
33	141.3	W	γ(422)
34	149.8	W	-

TABLE XXVII

2θ Angles, Intensities, and Identities of Peaks

Specimen 18 (Ti 30a/o, Al 70a/o)

Peak No.	2θ Value Degrees	Intensity	Identity
1	21.7	M	γ(001)
2	28.1	W	-
3	32.4	W	$TiAl_3$
4	35.4	W	-
5	36.4	VW	-
6	39.1	VS	γ(111)-$TiAl_3$
7	42.9	W	$TiAl_3$
8	43.8	M	γ(002)
9	46.4	S	γ(200)
10	65.6	S	γ(202)-$TiAl_3$
11	66.8	W	γ(220)
12	67.6	M	γ(212)
13	75.1	W	γ(301)-$TiAl_3$
14	77.2	S	γ(113)
15	81.0	S	γ(131)
16	82.5	VW	$TiAl_3$
17	84.0	S	γ(222)
18	97.4	W	γ(004)
19	103.5	M	γ(223)
20	109.5	VW	γ(330)
21	111.2	W	$TiAl_3$
22	113.2	S	γ(313)-$TiAl_3$
23	114.4	M	γ(331)
24	117.2	M	-
25	120.9	M	$TiAl_3$
26	122.8	M	$TiAl_3$
27	136.3	M	-
28	144.9	M	-
29	151.6	M	γ(314)
30	157.6	M	γ(115)

TABLE XXVIII

2θ Angles, Intensities, and Identities of Peaks

Specimen 19 (Ti 25a/o, Al 70a/o, Zr 5a/o)

Peak No.	2θ Value Degrees	Intensity	Identity
1	21.4	S	γ(001)
2	31.9	W	γ(110)
3	35.2	W	-
4	38.8	VS	γ(111)
5	43.5	M	γ(002)
6	45.9	S	γ(200)
7	51.0	W	γ(201)
8	54.8	W	$TiAl_3$
9	60.2	VW	-
10	65.0	S	γ(202)-$TiAl_3$
11	66.9	M	γ(212)
12	76.8	S	-
13	80.2	S	γ(131)
14	83.2	S	γ(222)-$TiAl_3$
15	96.2	W	γ(004)
16	102.4	W	γ(223)
17	105.6	W	γ(401)
18	106.9	W	$TiAl_3$
19	110.2	VW	$TiAl_3$
20	112.2	S	$TiAl_3$
21	113.5	W	γ(313)
22	115.7	M	γ(331)
23	119.5	M	γ(402)
24	121.0	W	$TiAl_3$
25	128.1	W	γ(332)
26	130.7	W	$TiAl_3$
27	134.8	M	γ(224)
28	142.2	M	-
29	150.0	W	-
30	151.7	W	γ(314)

Appendix E

Tabulation of Diffraction Data for Graphical Computation of Lattice Parameters

The accompanying tables (XXIX to XXXV) contain the computed data used in the graphs of Appendix F. The two values of a^2 and $(c/a)^2$ used to determine each line are indicated herein.

TABLE XXIX

Tabulated Values for Graphical Determination of Lattice Parameters

Specimen 8 (Ti 45a/o, Al 55a/o)

Note: 2θ Values are corrected for calibration error

Peak No.	Plane	2θ Deg.	Sinθ	$\frac{4\sin^2\theta}{\lambda^2 1^2}$	$\frac{h^2 + k^2}{1^2}$
1	113	78.06	.62973	.07427	0.22222
2	131	79.54	.63971	.68976	10.0
3	313	112.90	.83340	.13008	1.1111
4	224	137.42	.93175	.09146	0.5000
5	422	141.05	.94282	.37457	5.0

Peak No.	Equation of line	$(a/c)^2$	a^2	$(a/c)^2$	a^2
1	$(a/c)^2 = 0.07427a^2 - 0.22222$	.952	15.811	.950	15.784
2	$(a/c)^2 = 0.68976a^2 - 10.0$	.952	15.878	.950	15.875
3	$(a/c)^2 = 0.13008a^2 - 1.1111$	.952	15.861	.950	15.845
4	$(a/c)^2 = 0.09146a^2 - 0.5000$	.952	15.876	.950	15.855
5	$(a/c)^2 = 0.37457a^2 - 5.0$	.952	15.8904	.950	15.885

TABLE XXX

Tabulated Values for Graphical Determination of Lattice Parameters

Specimen 9 (Ti 42.5a/o, Al 55a/o, Zr 2.5a/o)

Note: 2θ Values are corrected for calibration error

Peak No.	Plane	2θ Deg.	Sinθ	$\frac{4\sin^2\theta}{\lambda^2 1^2}$	$\frac{h^2 + k^2}{1^2}$
1	113	77.77	.62783	.07382	0.22222
2	131	79.30	.63810	.68629	10.0
3	222	83.05	.66301	.18523	2.0
4	313	112.42	.83108	.12935	1.11111
5	224	137.00	.93042	.09119	0.50

Peak No.	Equation of line	$(a/c)^2$	a^2	$(a/c)^2$	a^2
1	$(a/c)^2 = 0.07382a^2 - 0.22222$	.950	15.879	.960	16.015
2	$(a/c)^2 = 0.68629a^2 - 10.0$	.950	15.955	.960	15.970
3	$(a/c)^2 = 0.18523a^2 - 2.0$	.950	15.926	.960	15.980
4	$(a/c)^2 = 0.12935a^2 - 1.11111$	.950	15.934	.960	16.012
5	$(a/c)^2 = 0.09119a^2 - 0.50$	.950	15.900	.960	16.010

TABLE XXXI

Tabulated Values for Graphical Determination of Lattice Parameters

Specimen 10 (Ti 40a/o, Al 55a/o, Zr 5a/o)

Note: 2θ Values are corrected for calibration error

Peak No.	Plane	2θ Deg.	Sinθ	$\frac{4\sin^2\theta}{\lambda^2 l^2}$	$\frac{h^2 + k^2}{l^2}$
1	113	77.60	.62660	.07353	0.22222
2	131	79.29	.63796	.68599	10.0
3	222	82.96	.66236	.18487	2.0
4	313	112.15	.82982	.12896	1.1111
5	224	136.02	.92725	.09057	0.50

Peak No.	Equation of line	$(a/c)^2$	a^2	$(a/c)^2$	a^2
1	$(a/c)^2 = 0.07353a^2 - 0.22222$	.950	15.942	.958	16.051
2	$(a/c)^2 = 0.68599a^2 - 10.0$	.950	15.962	.958	15.974
3	$(a/c)^2 = 0.18487a^2 - 2.0$	.950	15.957	.958	16.001
4	$(a/c)^2 = 0.12896a^2 - 1.1111$	.950	15.983	.958	16.045
5	$(a/c)^2 = 0.09057a^2 - 0.50$	.950	16.009	.958	16.097

TABLE XXXII

Tabulated Values for Graphical Determination of Lattice Parameters

Specimen 11 (Ti 37.5a/o, Al 55a/o, Zr 7.5a/o)

Note: 2θ Values are corrected for calibration error

Peak No.	Plane	2θ Deg.	Sinθ	$\frac{4\sin^2\theta}{\lambda^2 l^2}$	$\frac{h^2 + k^2}{l^2}$
1	131	78.80	.63473	.67906	10.0
2	222	82.41	.65869	.18282	2.0
3	313	111.67	.82747	.12831	1.1111
4	402	117.45	.85473	.30784	4.0
5	422	138.17	.93414	.36770	5.0
6	115	147.42	.98064	.06484	.080

Peak No.	Equation of line	$(a/c)^2$	a^2	$(a/c)^2$	a^2
1	$(a/c)^2 = 0.67906a^2 - 10.0$	.960	16.140	.970	16.154
2	$(a/c)^2 = 0.18282a^2 - 2.0$	.960	16.190	.970	16.245
3	$(a/c)^2 = 0.12831a^2 - 1.1111$	.960	16.141	.970	16.219
4	$(a/c)^2 = 0.30784a^2 - 4.0$	.960	16.112	.970	16.145
5	$(a/c)^2 = 0.36770a^2 - 5.0$	.960	16.209	.970	16.236
6	$(a/c)^2 = 0.06484a^2 - 0.08$	.960	16.040	.970	16.194

TABLE XXXIII

Tabulated Values for Graphical Determination of Lattice Parameters

Specimen 12 (Ti 35a/o, Al 55a/o, Zr 10a/o)

Note: 2θ Values are corrected for calibration error

Peak No.	Plane	2θ	Sinθ	$\frac{4\sin^2\theta}{\lambda^2 1^2}$	$\frac{h^2 + k^2}{1^2}$
1	113	76.99	.62238	.07254	0.22222
2	131	78.63	.63365	.67675	10.0
3	313	110.97	.82393	.12714	1.1111
5	402	116.64	.85099	.30515	4.0
6	005	137.34	.93150	.05850	0.0

Peak No.	Equation of line	$(a/c)^2$	a^2	$(a/c)^2$	a^2
1	$(a/c)^2 = 0.07254a^2 - 0.22222$	.944	16.076	.950	16.159
2	$(a/c)^2 = 0.67675a^2 - 10.0$	.944	16.171	.950	16.180
3	$(a/c)^2 = 0.12714a^2 - 1.1111$	.944	16.165	.950	16.212
5	$(a/c)^2 = 0.30515a^2 - 4.0$	.944	16.202	.950	16.221
6	$(a/c)^2 = 0.05850a^2$	.944	16.137	.950	16.239

TABLE XXXIV

Tabulated Values for Graphical Determination of Lattice Parameters

Specimen 13 (Ti 40a/o, Al 60a/o)

Note: 2θ Values are corrected for calibration error

Peak No.	Plane	2θ Deg.	Sinθ	$\frac{4\sin^2\theta}{\lambda^2 1^2}$	$\frac{h^2 + k^2}{1^2}$
1	113	78.63	.63365	.07520	0.22222
2	313	113.50	.83629	.13098	1.11111
3	402	118.92	.86127	.31257	4.0
4	224	138.80	.93612	.09232	0.5
5	422	141.35	.94363	.37521	5.0

Peak No.	Equation of line	$(a/c)^2$	a^2	$(a/c)^2$	a^2
1	$(a/c)^2 = 0.07520a^2 - 0.22222$	.970	15.855	.980	15.988
2	$(a/c)^2 = 0.13098a^2 - 1.11111$	.970	15.889	.980	15.965
3	$(a/c)^2 = 0.31257a^2 - 4.0$	.970	15.900	.980	15.932
4	$(a/c)^2 = 0.09232a^2 - 0.5$	.970	15.924	.980	16.032
5	$(a/c)^2 = 0.37521a^2 - 5.0$	.970	15.911	.980	15.938

TABLE XXXV

Tabulated Values for Graphical Determination of Lattice Parameters

Specimen 14 (Ti 35a/o, Al 60a/o, Zr 5a/o)

Note: 2θ Values are corrected for calibration error

Peak No.	Plane	2θ Deg.	Sinθ	$\frac{4\sin^2\theta}{\lambda^2 1^2}$	$\frac{h^2 + k^2}{1^2}$
1	113	77.42	.62538	.07325	0.22222
2	131	79.53	.63957	.68946	10.0
3	222	83.06	.66301	.18523	2.0
4	004	97.14	.74976	.05922	0.0
5	402	118.41	.85896	.31090	4.0
6	422	140.40	.94088	.37303	5.0

Peak No.	Equation of line	$(a/c)^2$	a^2	$(a/c)^2$	a^2
1	$(a/c)^2 = 0.07325a^2 - 0.22222$	.940	15.868	.934	15.786
2	$(a/c)^2 = 0.68946a^2 - 10.0$	.940	15.868	.934	15.859
3	$(a/c)^2 = 0.18523a^2 - 2.0$	.940	15.872	.934	15.840
4	$(a/c)^2 = 0.05922a^2$	.940	15.875	.934	15.772
5	$(a/c)^2 = 0.31090a^2 - 4.0$	.940	15.890	.934	15.870
6	$(a/c)^2 = 0.37303a^2 - 5.0$	.940	15.924	.934	15.908

TABLE XXXVI

Tabulated Values for Graphical Determination of Lattice Parameters

Specimen 15 (Ti 30a/o, Al 60a/o, Zr 10a/o)

Note: 2θ Values are corrected for calibration error

Peak No.	Plane	2θ Deg.	Sinθ	$\frac{4\sin^2\theta}{\lambda^2 1^2}$	$\frac{h^2 + k^2}{1^2}$
1	113	76.85	.62142	.07232	0.22222
2	131	78.93	.63567	.68107	10.0
3	222	82.46	.65895	.18297	2.0
4	400	100.27	.76761	-	-
5	313	110.07	.82442	.12729	1.11111
6	331	113.24	.83504	1.17529	18.0

Peak No.	Equation of line	$(a/c)^2$	a^2	$(a/c)^2$	a^2
1	$(a/c)^2 = 0.07232a^2 - 0.22222$	.936	16.015	.940	16.071
2	$(a/c)^2 = 0.68107a^2 - 10.0$	.936	16.057	.940	16.063
3	$(a/c)^2 = 0.18297a^2 - 2.0$	.936	16.0465	.940	16.068
4	$a^2 = 16.110$	Vertical Line			
5	$(a/c)^2 = 0.12729a^2 - 1.11111$	.936	16.083	.940	16.114
6	$(a/c)^2 = 1.17529a^2 - 18.0$	.936	16.112	.940	16.115

Appendix F

Graphical Determination of Lattice Parameters

Fig. 14 through 21 show the lattice parameters of the gamma phase as determined by graphical methods. The graph of specimen 11 (Fig. 17) resulted in an area of poor reliability and a median value was selected for determining the $(a/c)^2$ value.

The upper part of each chart contains the drift error which is given as $\frac{1}{2}\left(\frac{\cos^2\theta}{\sin\theta} + \frac{\cos^2\theta}{\theta}\right)$ and is simply labelled drift.

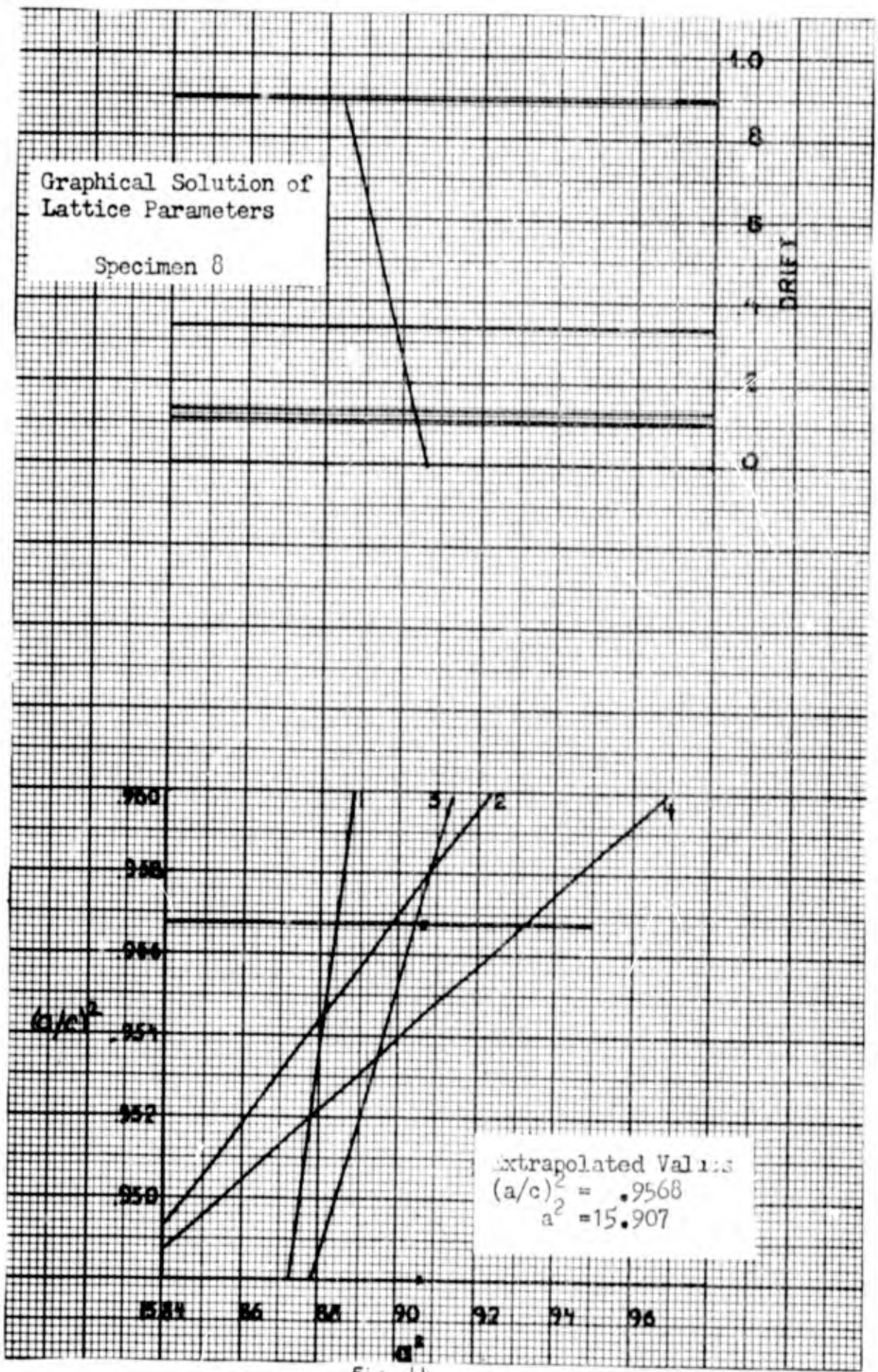
Graphical Solution of
Lattice Parameters
Specimen 8
1.0
8
6
4
2
0
DRIFT
950
948
946
944
942
940
$(a/c)^2$
1
3
2
4
Extrapolated Values
$(a/c)^2$ = .9568
a^2 = 15.907
84
86
88
90
92
94
96
a^2

Fig. 14

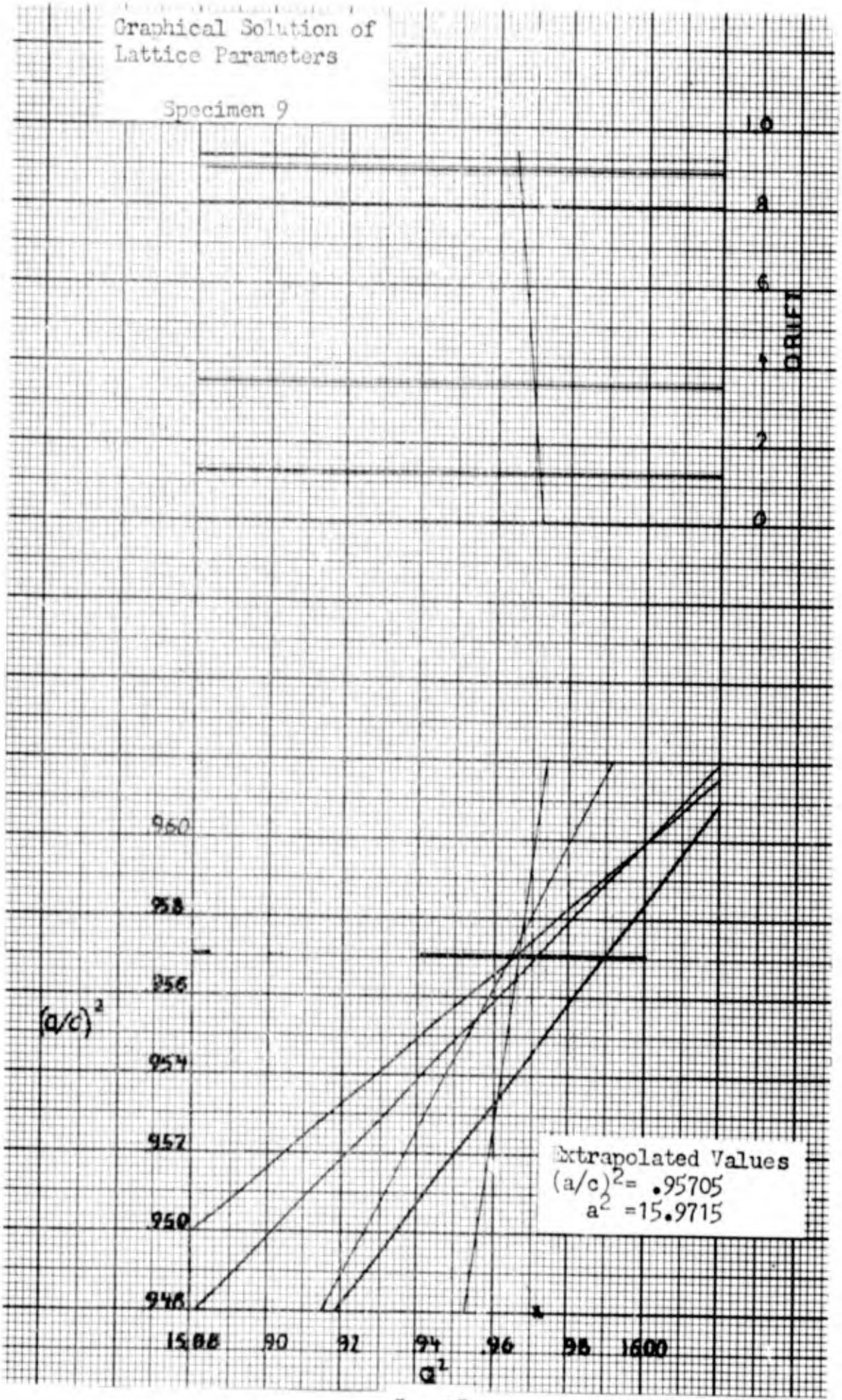
Graphical Solution of
Lattice Parameters
Specimen 9
DRIFT
10
8
6
4
2
0
960
958
956
954
952
950
948
(a/c)²
15.88
90
92
94
96
98
1600
Q²
Extrapolated Values
(a/c)²= .95705
a² =15.9715

Fig. 15

CAW/Mech 62-16

Graphical Solution of Lattice Parameters

Specimen 10

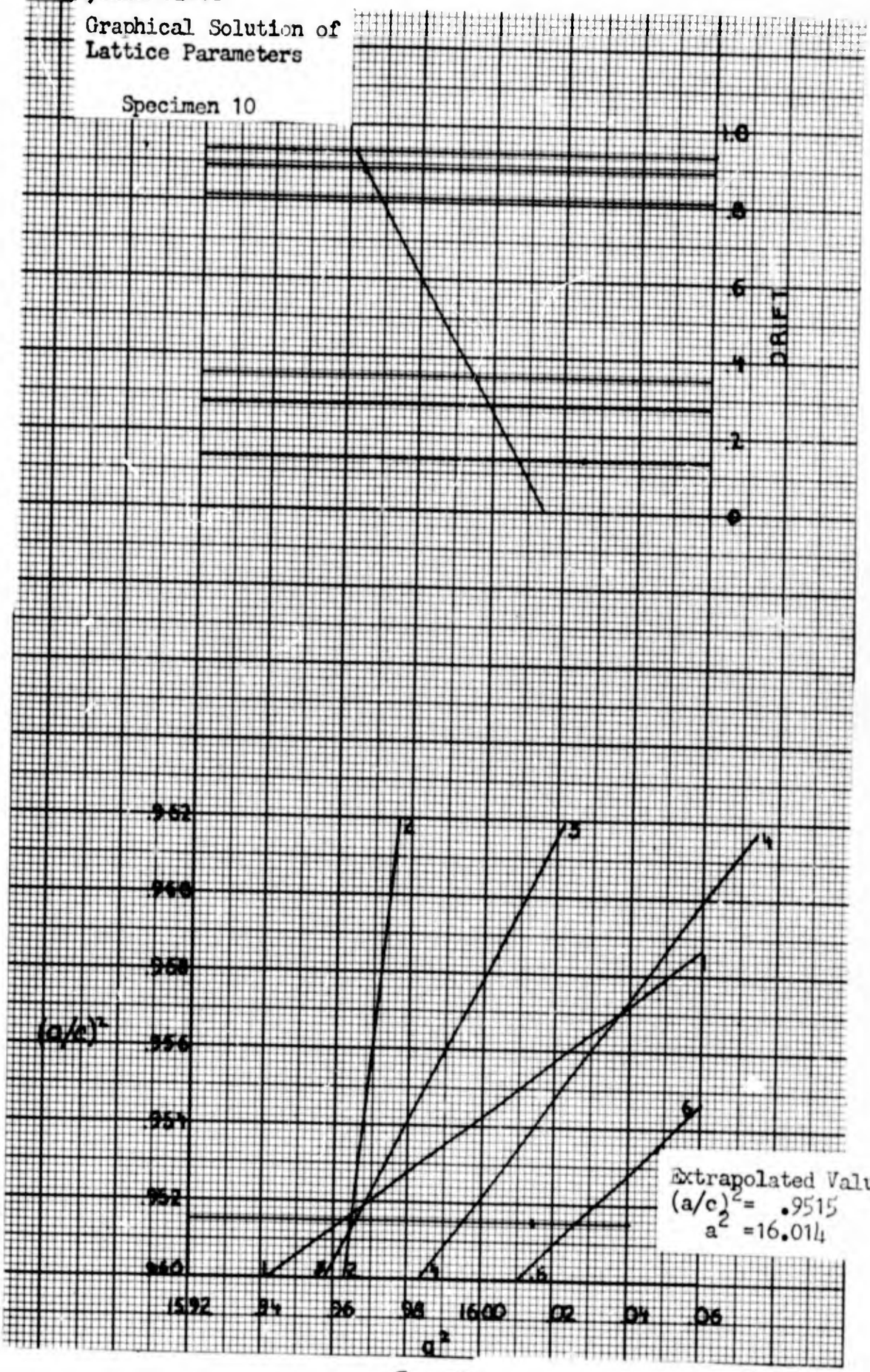

Extrapolated Values
$(a/c)^2 = .9515$
$a^2 = 16.014$

Fig. 16

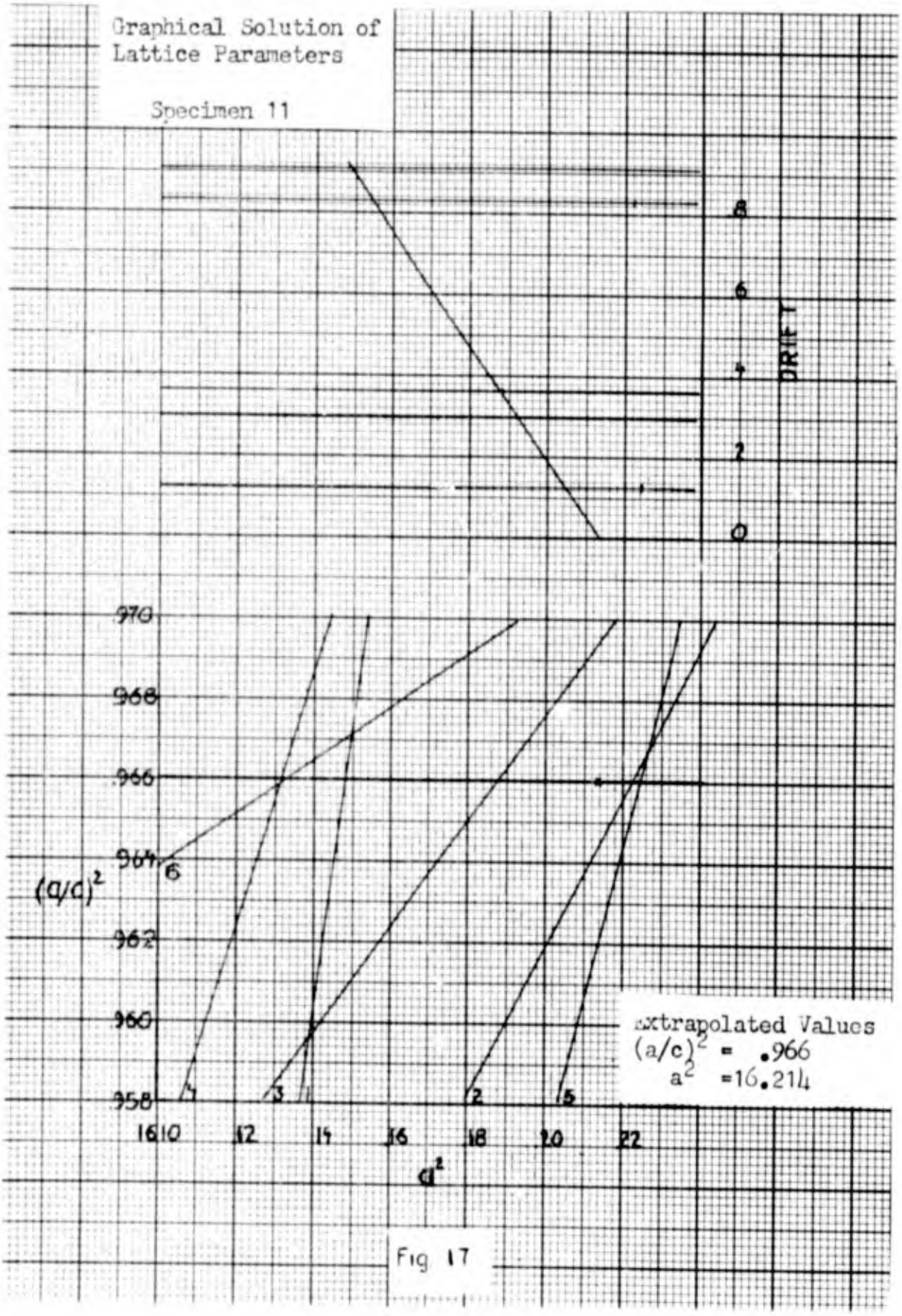
Graphical Solution of
Lattice Parameters
Specimen 11
DRIFT
8
6
4
2
0
970
968
966
964
962
960
958
$(a/c)^2$
6
4
3
1
2
5
16
18
20
22
d^2
extrapolated Values
$(a/c)^2$ = .966
a^2 = 16.214

Fig 17

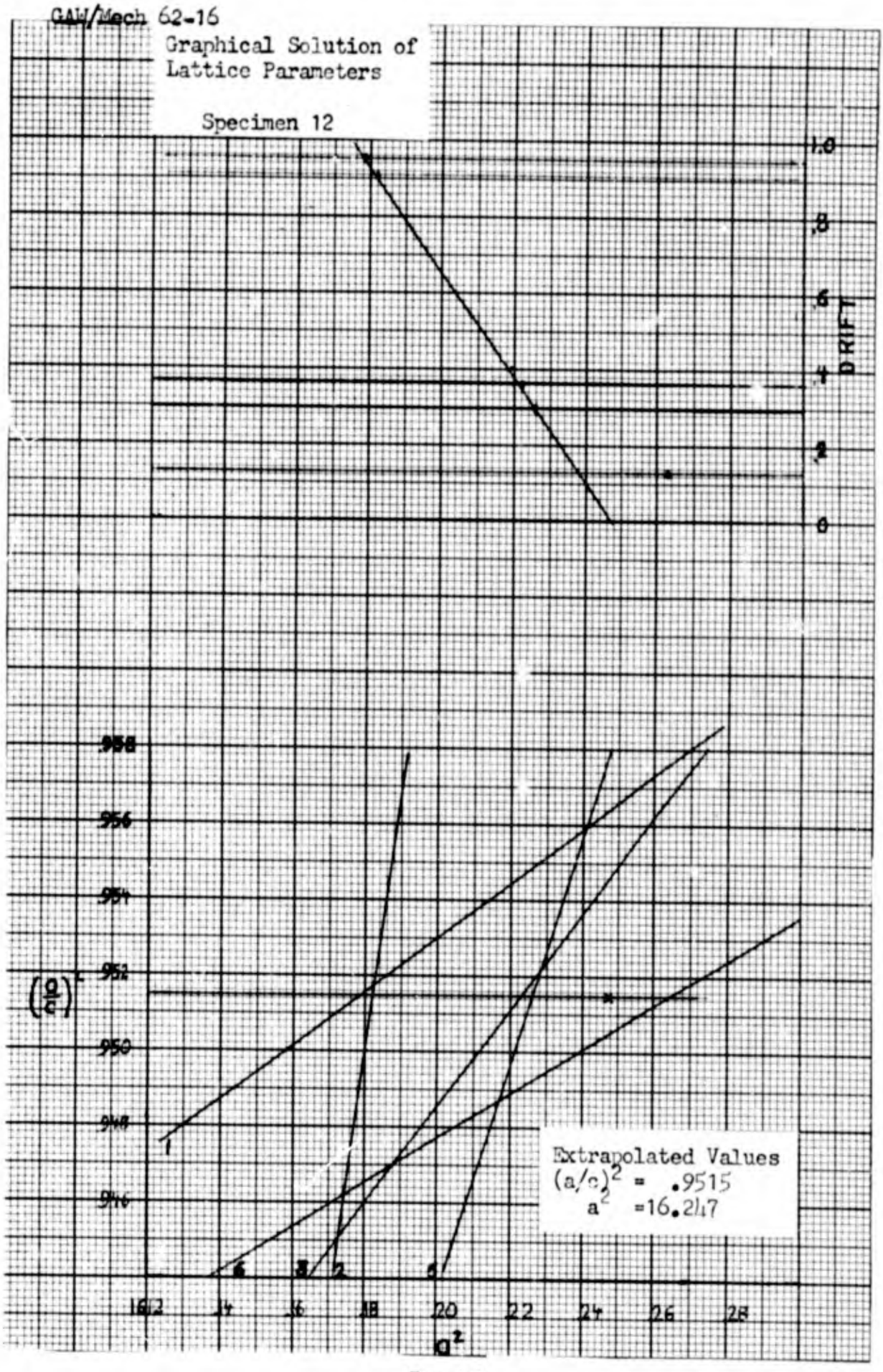
GAU/Mech 62-16
Graphical Solution of
Lattice Parameters
Specimen 12
DRIFT
1.0
.8
.6
.4
.2
0
$\left(\frac{a}{c}\right)^2$
958
956
954
952
950
948
946
Extrapolated Values
$(a/c)^2$ = .9515
a^2 =16.247
16.2
18
20
22
24
26
28
a^2

Fig. 18

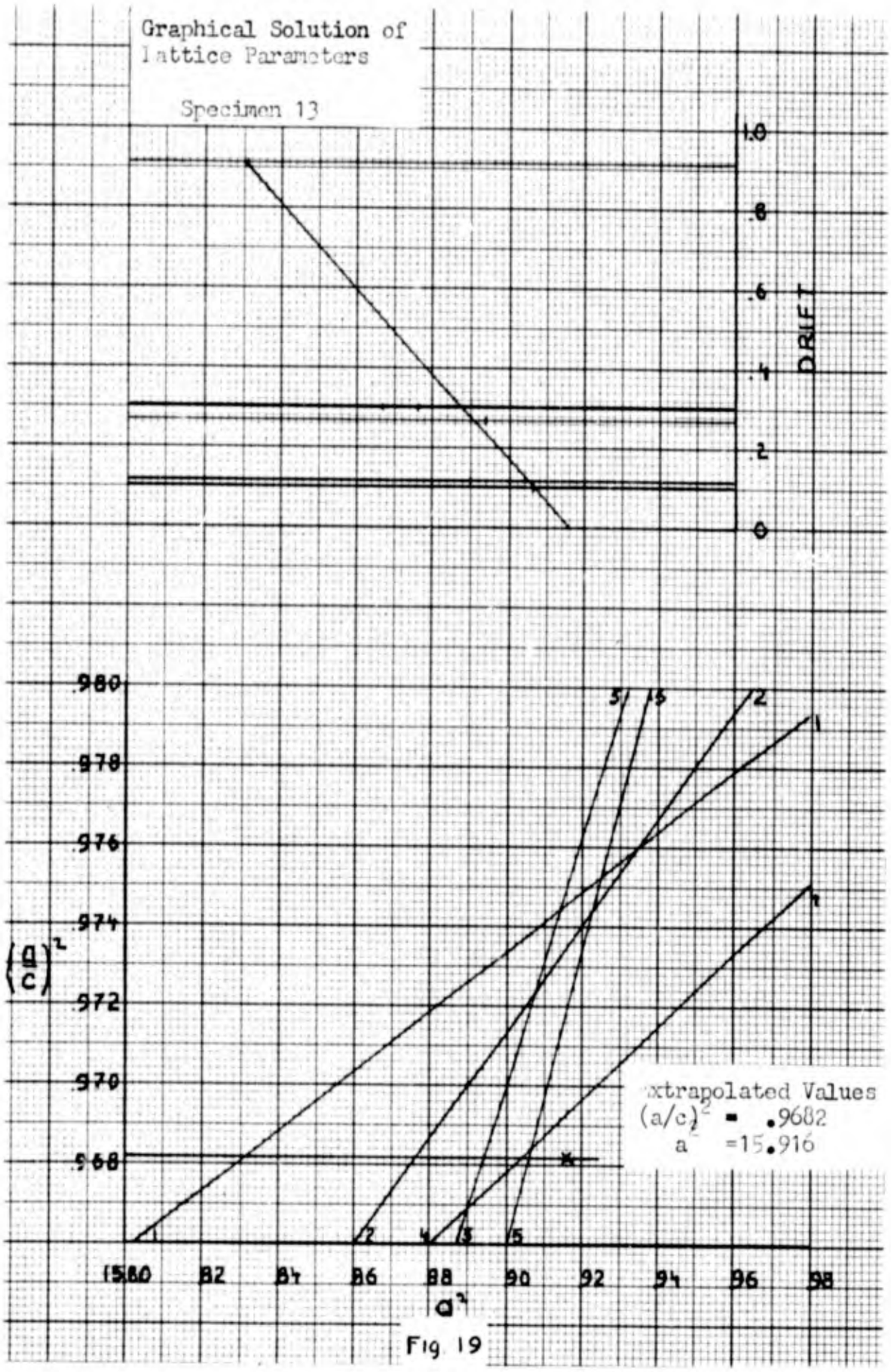
Graphical Solution of
Lattice Parameters
Specimen 13
DRIFT
1.0
.8
.6
.4
.2
0
.980
.978
.976
.974
.972
.970
.968
(a/c)²
1580
82
84
86
88
90
92
94
96
98
a²
Extrapolated Values
(a/c)² = .9682
a = 15.916

Fig 19

GAW/Mech 62-16

Graphical Solution of
Lattice Parameters

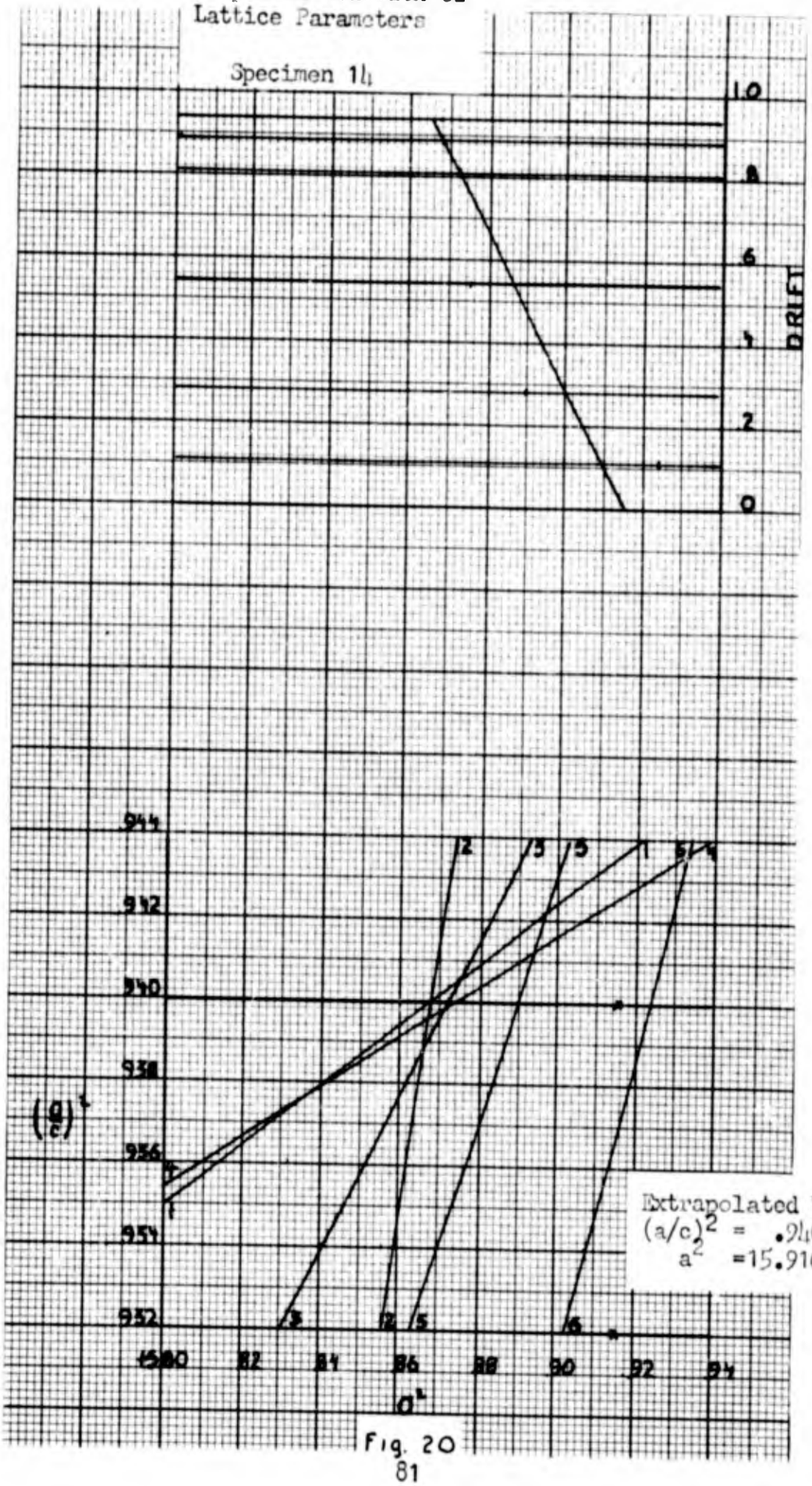

Fig. 20

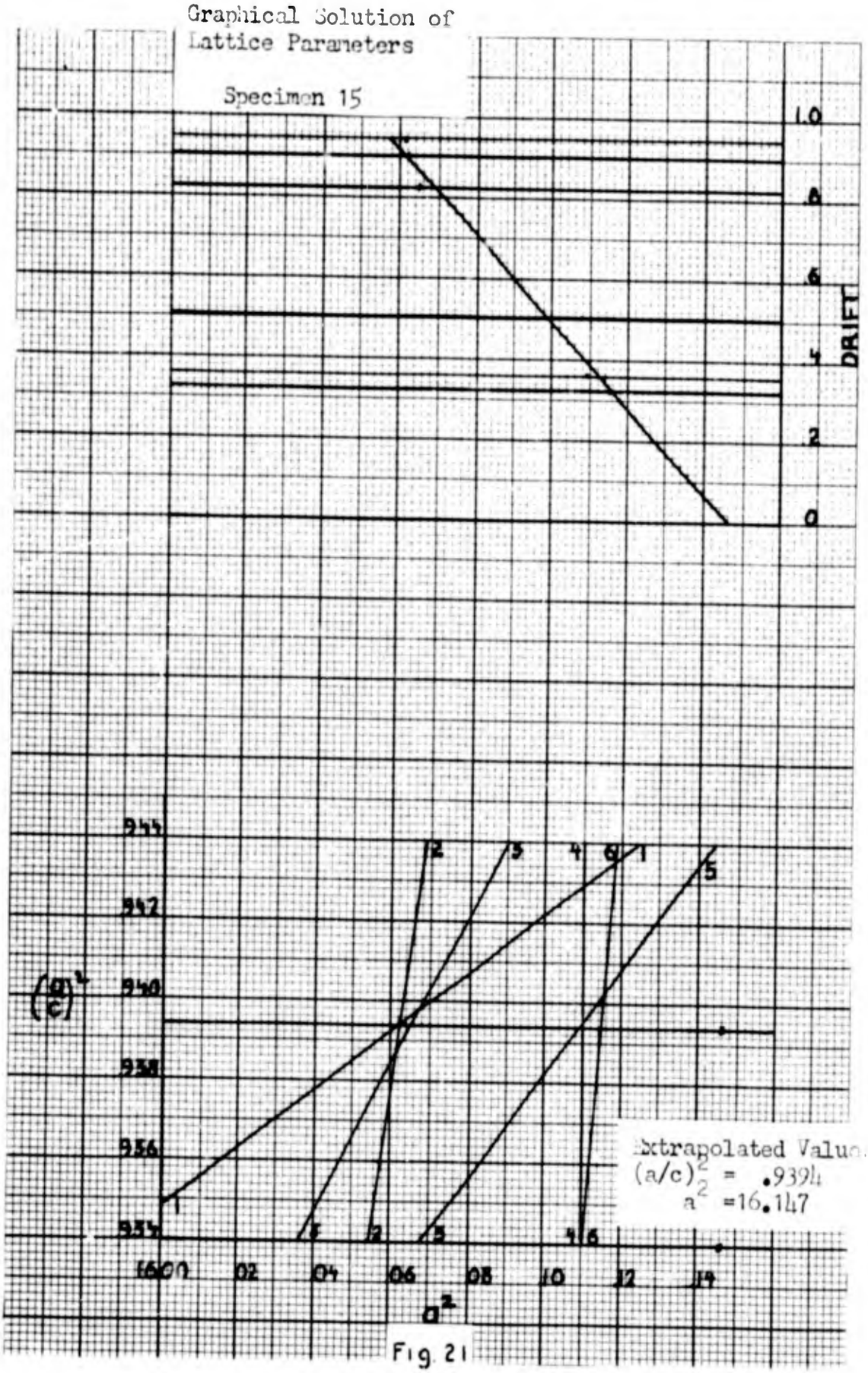
Graphical Solution of
Lattice Parameters
Specimen 15
DRIFT
1.0
.8
.6
.4
.2
0
$(\frac{a}{c})^2$
.944
.942
.940
.938
.936
.934
1600
02
04
06
08
10
12
14
a^2
Extrapolated Value
$(a/c)^2$ = .9394
a^2 = 16.147

Fig. 21

Appendix G

Photomicrographs

The photomicrographs in this section generally support the phase determination. Fig. 22 shows the microscopic cracks that developed in the specimens during their preparation.

The photographs taken by Mr. Harich at the University of Dayton Research Institute are identified by the letters "UD" located under the lower right hand corner of the photograph.

The photomicrographs of specimens 14 and 18 were taken in the as-melted condition, as mentioned in Section II, and were not considered in determining the phase.

Fig. 22

Specimen 16 (Ti 35a/o, Al 65a/o) showing cracks in micrstructure. Heated at 2280°F for 25.5 hrs. Water quenched. Polarized light. 400X.

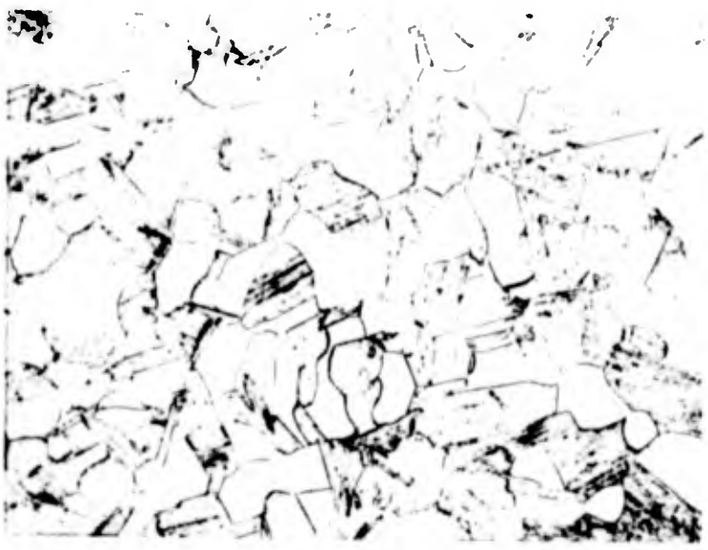

Fig. 23

Specimen 1 (Ti 50a/o, Al 50a/o). Heat treated at 2500°F for 23.6 hrs. X-ray shows two phases present. 250X. UD

Fig. 24

Specimen 5 (Ti 40a/o, Al 50a/o, Zr 10a/o). Heat treated at 2350°F for 24 hrs. Water quenched. X-ray indicates two phases present. 250X. UD

Fig. 25

Specimen 6 (Ti 37.5a/o, Al 50a/o, Zr 12.5a/o). Heat treated at 2350°F for 24 hrs. Water quenched. X-ray indicates two phases present. 250X. UD

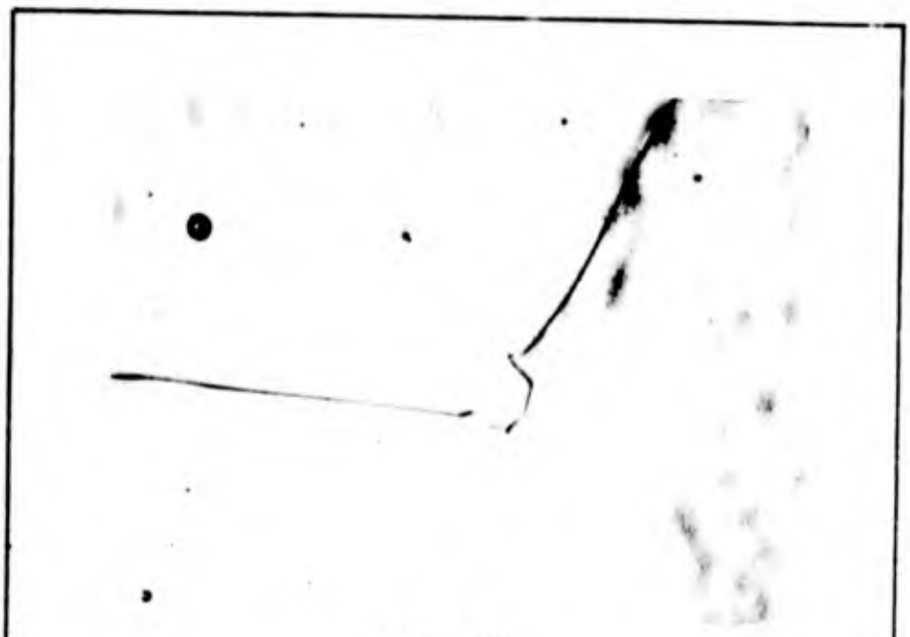

Fig. 26

Specimen 8 (Ti 45a/o, Al 55a/o). Heat treated at 2360°F for 23.8 hrs. Water quenched. Single phase . 250X

UD

Fig. 27

Specimen 9 (Ti 42.5a/o, Al 55a/o, Zr 2.5a/o). Heat treated at 2360°F for 23.8 hrs. Water quenched. Single phase . 250X.

UD

Fig. 28

Specimen 11 (Ti 37.5a/o, Al 55a/o, Zr 7.5a/o). Heat treated at 2320°F for 24 hrs. Water quenched. Single phase . 250X. UD

Fig. 29

Specimen 12 (Ti 35a/o, Al 55a/o, Zr 10a/o). Heat treated at 2320°F for 24 hrs. Water quenched. X-ray indicates two phases present. 250X. UD

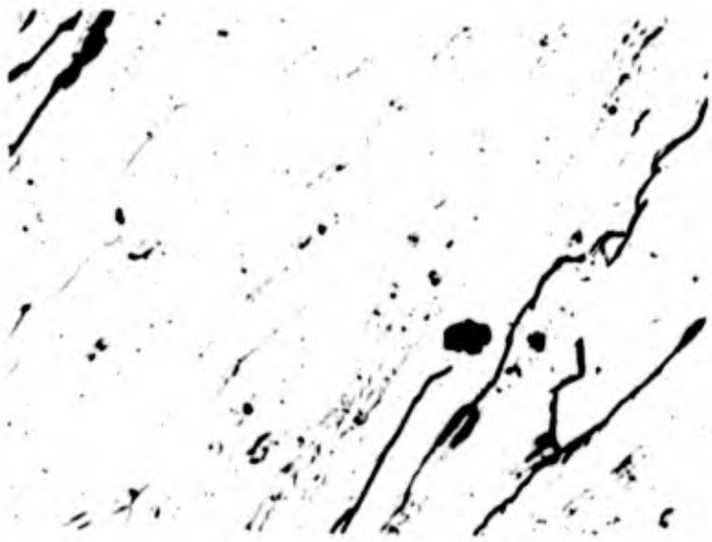

Fig. 30

Specimen 14 (Ti 35a/o, Al 60a/o, Zr 5a/o). As melted. 250X.

UD

Fig. 31

Specimen 18 (Ti 30a/o, Al 70a/o). As melted. 250X.

UD

GAW/Mech 62-16

Vita

Duane Hardy Troup [redacted] He attended Colman Public Schools graduating in 1941. After one and one-half years of college at South Dakota State College, Brookings, South Dakota, he was called to active duty to take flight training. Completing flight training he received a commission as Second Lieutenant in the Army Air Corps in May 1944. After receiving 5 months of advanced flight training, including bombing and gunnery, he went to the CBI theater where he remained until the close of World War II. Released from active duty in December 1945, he enrolled in Aeronautical Engineering at the University of Minnesota, graduating with the degree of Bachelor of Aeronautical Engineering in June 1948. Recalled to active duty in July 1948 to attend Weather Officer Training, he acted in that capacity until his assignment at the Air Force Institute of Technology.

[redacted]

This thesis was typed by Mrs. Patricia K. Troup